UNIVERSITÀ DEGLI STUDI DI PADOVA

Dipartimento di Fisica e Astronomia "Galileo Galilei"
Master Degree in Astrophysics and Cosmology

Final dissertation

Analysis of the variability properties of the stars in the PLATO Input Catalogue

Thesis supervisor

Prof. Giampaolo Piotto

Thesis co-supervisor

Dr. Marco Montalto

Thesis external examiner

Dr. Silvano Desidera

Candidate

Adriana Barbieri

18/10/2023

Academic Year 2022/2023

Analysis of the variability properties of the stars in the PLATO Input Catalogue

Adriana Barbieri

Abstract

PLATO (PLAnetary Transits and Oscillations of stars) is the European Space Agency (ESA)'s mission scheduled for 2026 with the core goal to find and characterize rocky planets in the habitable zone of solar-like stars. In the first public release of the all-sky PLATO Input Catalogue (asPIC1.1) the stellar samples optimised for the mission's scientific requirements have been defined and they include M dwarfs and FGK dwarf and subgiant target stars. The final observing strategy will be settled two years before launch; the optimal PLATO sky fields will be those that maximize the number of the most suitable targets for the detection of transiting exoplanets.

This work aims to evaluate the variability (intrinsic and extrinsic) of PLATO targets, in order to characterise them before the final sky fields and targets selection.

We exploited the largest whole-sky variability analysis to date based on coherent photometric, astrometric, and spectroscopic data from the third data release of ESA's Gaia mission, Gaia DR3. We cross-matched by the unique identifier *source_id* all the PIC sources included in two wide sky regions at ecliptic latitudes $|\beta| > 38°$, which envelope every allowed choice of the PLATO sky fields, with the Gaia DR3 variable sources categorized into 11 specific classes.

From this operation it resulted that the sources included in the considered sub-samples from the PLATO Input Catalogue can be distinguished into the following variability types: planetary transits hosts, short-timescale variables, eclipsing binaries, solar-like stars, upper Main Sequence oscillators, RR Lyrae stars, Cepheids and long period variables. Their properties have been investigated and the light-curves for exemplary sources from each variability class have been extracted, showing the pulsating, rotating or binary nature of the targets.

We furthermore focused on the relevance of these sources for the PLATO space mission (in relation to both the primary objectives and the complementary science) and for future research prospects.

To my mum Patrizia, my dad Giuseppe, and my brothers Alessandro and Edoardo.

Acknowledgements

This work has made use of data from the European Space Agency (ESA) mission *Gaia* processed by the *Gaia* Data Processing and Analysis Consortium (DPAC, `https://www.cosmos.esa.int/web/gaia/dpac/consortium`).
Funding for the DPAC has been provided by national institutions, in particular the institutions participating in the *Gaia* Multilateral Agreement.
The Gaia mission website is `https://www.cosmos.esa.int/gaia`, the Gaia archive website is `https://archives.esac.esa.int/gaia`.
This work presents results from the ESA space mission PLATO. The PLATO payload, the PLATO Ground Segment and PLATO data processing are joint developments of ESA and the PLATO Mission Consortium (PMC). Funding for the PMC is provided at national levels, in particular by countries participating in the PLATO Multilateral Agreement. Members of the PLATO Consortium can be found at `https://platomission.com/`. The ESA PLATO mission website is `https://www.cosmos.esa.int/plato`.
The all-sky PLATO Input Catalogue (asPIC1.1) is available in electronic form at MAST[1] as a High Level Science Product via `https://dx.doi.org/10.17909/t9-8msm-xh08` and `https://archive.stsci.edu/hlsp/aspic`, in the SSDC[2] tools page `https://tools.ssdc.asi.it/asPICtool/` and at the CDS[3] via `https://cdsarc.u-strasbg.fr/viz-bin/cat/J/A+A/653/A98`. The PIC sources object of this thesis work have been kindly provided by Dr. Montalto via a private communication.
This work has made use of the SIMBAD database (`https://simbad.cds.unistra.fr/simbad/`) operated at CDS, of the graphical viewer and editor TOPCAT (`https://www.star.bristol.ac.uk/mbt/topcat/`), of the open source environment Spyder (`https://www.spyder-ide.org/`) and of the open source LaTeX editor Overleaf (`https://it.overleaf.com`).

I am deeply grateful to Professor Giampaolo Piotto, Dr. Marco Montalto and Dr. Silvano Desidera of the University of Padova for the precise and invaluable support provided during the course of this thesis work.
I would also like to express my sincere appreciation to my family and my friends for their encouragement throughout my studies.

[1] Mikulski Archive for Space Telescopes (MAST) at the Space Telescope Science Institute. STScI is operated by the Association of Universities for Research in Astronomy, Inc., under NASA contract NAS5–26555. Support to MAST for these data is provided by the NASA Office of Space Science via grant NAG5–7584 and by other grants and contracts.

[2] Space Science Data Center, managed by the Italian Space Agency, ASI.

[3] Centre de Données astronomiques de Strasbourg (Strasbourg astronomical Data Center).

Contents

List of Figures

List of Tables

Introduction

. . . for had we never seen the stars, and the sun, and the heaven, none of the words which we have spoken about the universe would ever have been uttered. But now the sight of day and night, and the months and the revolutions of the years, have created number, and have given us a conception of time, and the power of enquiring about the nature of the universe. . .

Plato, in Timaeus

The first ground-breaking discovery of an exoplanet orbiting a solar-type star has occurred only in 1995 and has earned Michel Mayor and Didier Queloz the 2019 Nobel Prize in Physics. In the past 28 years, astronomers have discovered more than 5000 exoplanets[4], with the overwhelming majority orbiting solar-like stars, through ground based observatories and space telescopes.

The European Space Agency's PLATO mission, which benefits from a huge Italian contribution and will begin its exoplanetary hunt in 2026, will confirm European science at the forefront of exoplanet research.

PLATO prime mission goals are to detect and characterize thousands of extrasolar transiting planets of diverse sizes and orbital architectures in a wide range of systems, including Earth-

[4]The current count of confirmed planets in the NASA Exoplanet Archive (`https://exoplanetarchive.ipac.caltech.edu/index.html`), up to the 25th September 2023, is 5523.

sized planets up to the habitable zone of solar-type bright stars, and to investigate seismic activity in stars, enabling the precise characterisation of the planets host stars, particularly their age.
PLATO is set to work in close synergies with past (Kepler/K2), current (TESS, Gaia, CHEOPS, JWST) and future observatories (Ariel, E-ELT). The interface between PLATO and Gaia is particularly powerful, due to the latter survey providing astrometric data of unprecedented quality and quantity: indeed Gaia allows characterisation of the PLATO fields, enables the selection of PLATO target host stars, providing detailed properties for all of them, and has the potential to find giant transiting planets at intermediate separations around PLATO targets.

The Target/Field Characterization & Selection branch of the PLATO Mission Consortium (PMC) Science Management (PSM) is mainly composed by the researchers of the Exoplanet & Stellar Population Group of the "Galileo Galilei" Physics and Astronomy Department at the University of Padova. The Supervisor, co-Supervisor and External Examiner of the present Master thesis all belong to the PMC and carry out the research activities led towards the creation of the PLATO Input Catalogue (PIC), which is essential to the mission.

This work aims to study the variability properties of a sample of target stars included in the PIC and to discriminate between the different types of these variable sources according to Gaia classification, with a focus on their relevance for PLATO.

Finding and characterising extra-solar planets requires a detailed knowledge of the host stars. It is well known that the flux variability of host stars can interfere with the ability to reliably detect and confirm exoplanets; as a consequence it is of capital importance to assess and study the temporal variability of all PLATO sources and, when observing their lightcurves, discriminate between the presence of transiting exoplanets, star pulsations, magnetic activity and occultations/eclipses from stellar companions. Indeed stellar surface

inhomogeneities can impact planetary interpretations, and additionally, a significant source of false positive planetary transit signals may be due to blended eclipsing binaries nearby the target star, therefore astrophysical contaminants should be accounted for when looking for exoplanets signatures. Moreover, PLATO targets variability is interesting for scientific purposes beyond the mission core objectives: the Complementary Science program, among other tasks, will in fact assemble a comprehensive stellar variability catalogue based on the mission's foreseen unique database of variable phenomena.

This thesis is organized as follows. In Chapter 1 we present the PLATO space mission, with an overview on the mission design, the spacecraft payload and its scientific objectives and legacy. We introduce the PLATO Input Catalogue and we describe the requirements leading to the choice of the mission observing strategy and the sky fields, and to the selection and characterization of the current stellar targets. In Chapter 2 we provide a description of Gaia space mission, from its nominal design to its scientific objectives and achievements; we illustrate the content of its third data release (Gaia DR3) and we concentrate on its estensive variability analysis. In Chapter 3 we account for the cross-matching operation performed between PLATO targets and Gaia DR3 variable objects, and show the variability properties of the resulting eight different classes of variable sources. For each class, we present the all-sky distribution, the color-magnitude diagrams and the photometric time-series. In Chapter 4 we provide a brief summary of the present work, some concluding remarks and future perspectives. Finally, in Appendix A we detail the methods applied by the space missions Gaia and PLATO to detect and characterize the extra-solar planets and their host stars and in the Bibliography section we list the references for this work.

Chapter 1

PLATO space mission

1.1 Mission overview

The PLATO mission (PLAnetary Transits and Oscillations of stars) has been selected for the M3 mission launch foreseen in 2026 in the framework of the European Space Agency (ESA)'s Cosmic Vision 2015–2025 program[1].

It is a medium class transit survey mission which follows the recommendations of ESA's Exoplanet Roadmap Advisory Team (EPR-AT) [2] and whose core science goal is to detect and characterize extrasolar planets in order to reveal habitable worlds around solar-like stars (Rauer et al. 2014 [1], 2016 [2]).

PLATO will assemble the first catalogue of confirmed and characterised planets with known mean densities, compositions, and evolutionary stages, monitoring hundred thousands of bright stars[3] for up to 4 years (which can be extended to 8 years) to allow for an extensive radial-velocity follow-up program.

Its long-term legacy will be to identify statistically robust relations among planetary and stel-

[1] "Cosmic Vision 2015-2025" is the current cycle of ESA's long-term plan for space science missions, whose M-class (medium) missions are Solar Orbiter (M1), Euclid (M2), PLATO (M3), Ariel (M4) and EnVision (M5).

[2] EPR-AT was appointed by ESA with the purpose of advising the Agency on the best scientific and technological roadmap to pursue for the characterization of terrestrial exoplanets, up to the possible detection of biomarkers. The complete report "A European Roadmap for Exoplanets", published on 28 October 2010, is available at `https://sci.esa.int/s/wRe1blA` .

[3] $V < 11$ mag in the Johnson photometric visual band.

lar parameters and to reach a deep understanding of planetary systems' structure, formation and evolution, in analogy to the Hertzsprung–Russell diagram for stars.

The PLATO mission combines three measurement and analysis methods: photometric light curves to detect planetary transits and derive the planets radii with an accuracy of 3%, asteroseismic analysis of the obtained light curves to derive stellar masses and ages with 10% accuracy, and spectroscopic RV ground-based follow-up observations to provide the required planetary masses with a 10% accuracy.

Ground-based data, Gaia[4] results and asteroseismology from PLATO will be combined into one consistent analysis for a large number of stars of various masses and chemical compositions. Furthermore, many of the terrestrial planets in the habitable zone (HZ) of their host stars accurately characterized by PLATO will be key targets for spectroscopy of their atmospheres with JWST, E-ELT or dedicated future exoplanet spectroscopy satellites (e.g. ARIEL).

PLATO Complementary Science[5] (PLATO-CS) is entitled to 8% of the total PLATO mission telemetry budget and will be organized in the framework of a competitive guest observer's programme. It aims to exploit the full potential of the mission's unique database beyond the main scientific topics of exoplanet detection and stellar science for stars of spectral type later than F5. Among several objectives, it will deal with variable phenomena in the Universe and improve the state-of-the-art knowledge on Galactic Archeology.

[4]See next chapter on Gaia mission.

[5]See `https://fys.kuleuven.be/ster/research-projects/plato-cs`.

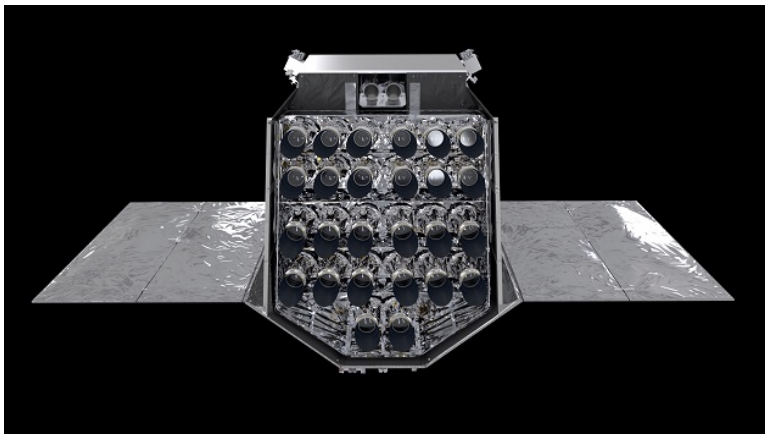

Figure 1.1: Artistic impression of PLATO spacecraft.
Credits: ESA.

1.1.1 Mission design

PLATO will be launched in 2026 from Kourou, ESA's spaceport in French Guiana, on an Arian 6 rocket[6] which will bring the satellite to the Earth-Sun L2 Lagrangian point[7].
After a commissioning phase the spacecraft will follow a large amplitude libration orbit around L2 and perform continuous observations with field rotation of 90° every 3 months for a nominal period of 4 years.

The current baseline operation strategy foresees a Long-duration Observation Phase (LOP) involving two continuous pointings lasting two years each; the covered LOP sky fields, located respectively in the northern and southern hemisphere, are devoted to the detection of planets with periods long enough to orbit in the habitable zone of solar-type stars (up to 1 year of orbital period).

In addition, the proposed "Step and stare" Observation Phase (SOP) can expand the total surveyed area up to 50% of the sky with shorter pointings of 2-5 months duration, and is devoted to shorter-period planet detections and different science cases such as galactic exploration.

[6]Further details about ESA's new launch vehicle can be found at `https://www.esa.int/Enabling_Support/Space_Transportation/Launch_vehicles/Ariane_6`

[7]L2 is placed approximately 1.5 million km from the Earth, along the Sun-Earth line in the direction opposite to the Sun.

The final selection of the targets and the observing strategy will be made two years before launch.

PLATO's primary data products will be made available in FITS format, and will consist in imagettes[8] of selected targets, parameters from transit photometry, asteroseismic analysis, stellar rotation and activity, high cadence optical light curves of large numbers of bright stars, a catalogue of fully characterised confirmed planetary systems and ground-based observation data.

ESA will establish a PLATO Mission Operations Centre (MOC) at the European Space Operations Centre (ESOC) in Darmstadt, Germany and a Science Operations Centre (SOC) at the European Space Astronomy Centre (ESAC) in Madrid, Spain, besides providing ground stations to ensure the necessary telecommanding and telemetry capabilities of the mission. In particular, the available data volume (or downlink capacity) transmitted by K- and X-band antenna is about 435 Gb on average per day.
The PLATO Mission Consortium (PMC)[9] is in charge of providing a PLATO Data Centre (PDC), a Science Management (PSM) Group, a Calibration/Operation Team (PCOT) and a Ground-Based Observations Programme (GOP) Team, that together with the MOC and the SOC constitute the mission's Science Ground Segment (SGS).

The PSM Group consists of five teams dealing with different research areas:

- Exoplanet science, led by Don Pollacco at the University of Warwick, UK.
- Stellar science, led by Marie-Jo Goupil at LESIA, Paris Observatory, France.
- Field / target characterisation and selection, led by Giampaolo Piotto at the University of Padova, Italy.
- Follow-up studies (GOP), led by Stephane Udry at Geneva Observatory, Switzerland.
- Complementary science, led by Conny Aerts at the University of Leuven, Belgium.

[8]Time series of flux values for each pixel inside the 6 x 6 px window aperture defined around the target star, that are downloaded to the ground in place of full CCD images, due to the mission's telemetry rate limitations.

[9]The PMC Science Management website can be found at `https://warwick.ac.uk/fac/sci/physics/research/astro/plato-science`

1.1.2 Instrumentation and payload

PLATO's spacecraft mainly consists of a Service Module (SVM) and a Payload Module (PLM). It has a launch mass of 2165 kg and measures in size about 3.4 m × 3.3 m × 3.8 m. The SVM includes a sun shield, a propulsion system, an attitude control system, a communication system, a thermal control system and a control and data management system[10].

The scientific payload consists of a common optical bench housing the on-board Data Processing System and 26 cameras, which are peculiar to the multi-telescope approach of the mission, relying on the principle of optical segmentation for a huge Field of View.

Each camera consists of a telescope optical unit, a focal plane assembly, a front-end electronic with its support structure, and related thermal equipment.

24 "normal" cameras are dedicated to scientific observations in broad band white light (500-1050 nm) of stars fainter than V = 8, with a read-out cadence of 25 seconds, while 2 "fast" cameras are dedicated to support the pointing stability performance of the spacecraft and to monitor very bright stars ($4 < V < 8$) in two different photometric bands (blue 505-700 nm, red 665-1050 nm) with a readout cadence of 2.5 seconds.

The normal cameras are arranged in 4 groups of six coaligned telescopes each; each camera in the same group shares the same instantaneous 1037 deg^2 FoV but the lines of sight of each group are offset by a 9.2 ° angle with respect to the z-axis of the payload module, in order to increase the total covered sky field up to 2232 deg^2, as shown in figure 1.2.

The 2 fast cameras pointing direction instead coincides with the center of the overall FoV.

The total focal plane array of PLATO counts 104 CCDs (4 detectors per camera) and each CCD is composed of 4510 × 4150 $pixels^2$ of 18 µm pixel size, with a pixel scale of 15 arcsec s^{-1}.

[10] Further details may be found at `https://platomission.com/`

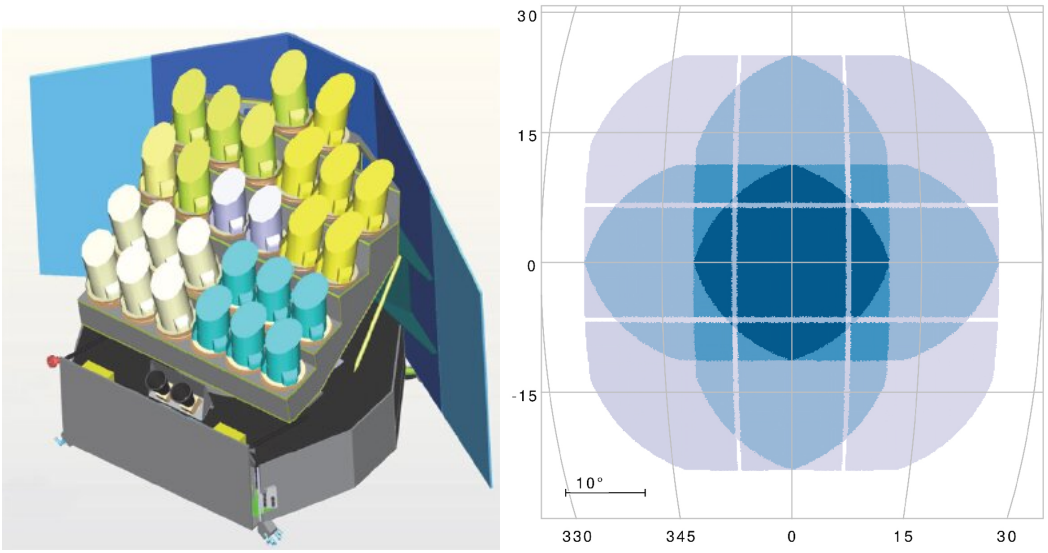

Figure 1.2: Left: design concept of PLATO spacecraft, showing the Payload Module, the Service Module and the Sun shield. Right: PLATO Field of View, where overlapping sky regions observed with 24, 18, 12 and 6 cameras are color coded with four shades of blue from dark to light.

1.1.3 Scientific objectives and legacy

As already stated, PLATO's main goal is to detect Earth-like planets in the habitable zone of solar-like stars.

The mission's other scientific objectives, as described in the PLATO Definition Study Report [3], are the following:

- Determine the bulk properties (mass, radius and mean density) of exoplanets in a wide range of systems, from terrestrial planets in the HZ of solar-like stars to gas giants and Neptune-sized planets.
- Study how planets and planetary systems evolve with age.
- Study the typical architectures of planetary systems.
- Analyse the correlation of planet properties and their frequencies with stellar parameters (e.g., stellar metallicity, stellar type).

- Analyse the dependence of the frequency of terrestrial planets on the environment in which they formed.
- Study the internal structure of stars by asteroseismology and its evolution with growing stellar age.
- Identify bright targets for spectroscopic follow-up measurements to investigate planetary atmospheres.

Moreover, PLATO will shed light on the uniqueness of our Solar System by detecting Earth Analog systems, will investigate rings, moons, Trojan asteroids and comets, and will ensure the detailed study of planet habitability by combining the knowledge of the planetary atmospheric properties and of their composition (to distinguish terrestrial planets from non-habitable gaseous mini-Neptunes).

The Complementary Science program will include topics like structure and evolution of Red Giant stars, hot OB sub-dwarf stars, massive stars, asymptotic giant branch stars and supergiants, white dwarfs, pre-main sequence stars and stellar clusters of various ages and metallicity.

Having the goal of measuring exoplanet transit radii with 3% precision, PLATO devotes a huge consideration in the determination of the stellar variability noise floor, that is composed of stellar flares, spots, oscillations and granulation. PLATO-CS will furthermore provide an unparalleled database of variable phenomena, with precision of the order of a few tens of ppm (parts-per-million) per hour for the brighter targets and ppt (parts-per-thousand) levels for much fainter objects, and on all time scales between seconds and years.
Other PLATO-CS Work Packages will deal with binary and multiple stars, pulsating stars, magnetic stars, rotational variables earlier than F5 class, stars with mass loss, Young Stellar Objects, stars with debris disks and transient phenomena.

1.2 PLATO Input Catalogue

The mission's telemetry limitations impose the pre-selection of the most suitable PLATO targets, since it is not possible to download full CCD images at a sufficient rate to detect planets.

The ultimate list of targets to be observed for each spacecraft pointing will be identified and compiled in the PLATO Input Catalogue (PIC), to be finalised two years between the mission launch, and whose building requires interfacing with large spectroscopic, photometric and astrometric input catalogues, including those from Kepler, TESS, and Gaia.

Establishing the properties of PLATO host stars is crucial to determine the properties of transiting planets; likewise, the optimal field selection is closely related to the target selection. The aim is to select observational fields that maximise the number of F5 or later spectral type dwarfs and subgiants; the benchmark case is the detection of an Earth-sized planet around a solar-like star (G0V star of V = 10) in 1 year period orbit, for which SNR > 10.

The Target / Field Characterisation & Selection branch of the PMC Science Management published in Montalto et al. 2021 [4] the first release of the all-sky PLATO Input Catalogue (known as asPIC1.1) based on Gaia Data Release 2 [11]; in Table B.1 of the mentioned paper a description of the columns content of the catalogue is provided.

The asPIC1.1 contains a total of 2 675 539 stars including FGK dwarfs and subgiants and M dwarfs; it is worth mentioning that since these samples are magnitude limited, hotter stars are more numerous than cool ones, because they are intrinsically more luminous. The overall uncertainties on the stellar parameters published in asPIC1.1 are $\sim$ 230 K (4%) for the effective temperatures, $\sim$ 0.1 R (9%) for the stellar radii, and $\sim$ 0.1 M (11%) for the stellar mass.

PIC will serve to:

- Identify the optimal PLATO Fields.
- Select the stellar samples.

[11] See Gaia Collaboration, Brown, et al (2018), DOI: `https://doi.org/10.1051/0004-6361/201833051` and the asPIC1.1 at `https://archive.stsci.edu/hlsp/aspic`.

- Characterize target stars as fully as possible, i.e. estimate their temperature, gravity, metallicity, size, variability, atmospheric activity, etc.
- Give a first estimate of the size of transiting objects.
- Assess field and source contaminants for PLATO targets.
- Optimize the Follow-Up strategy

1.2.1 Fields selection

To identify the optimal PLATO pointing fields is a demanding task, since it is necessary to simultaneously fulfill the mission scientific requirements, respect the geometrical constraints, maximize the scientific output of the mission and minimize the follow-up effort.
The ultimate PLATO LOP fields must host the required number of observable targets (with a goal of 15 000 F5-K7 dwarfs and subgiants brighter than V = 11 observed with a photometric precision better than 50 ppm in one hour), reduce interstellar extinction, avoid the expected rate of stellar contamination and false positives from blended eclipsing binaries, enable efficient ground based observations and reinforce the synergy with previous space missions such as TESS.
Moreover, in order to allow for a proper orientation of the spacecraft, the LOP fields must be centered at ecliptic latitudes $|\beta| > 63°$; therefore their centers must lie within the "allowed regions" showed in figure 1.3, which extend for 2750 deg^2 each and combined cover 11% of the sky area.
As a consequence, the outer regions enveloping every possible field choice with the aforementioned requirements extend for $|\beta| > 38°$, cover 38% of the whole sky and in an ecliptic reference frame look like wide polar caps. The vast majority of targets within the LOP outer envelopes can be optimally monitored by JWST.
The provisional long-duration phase fields LOPN1 (LOP field North 1) and LOPS1 (LOP field South 1) defined in Nascimbeni et al. 2022 [5] were located in the northern and southern hemispheres and centered on l = 81°.6, b = 24°.6 (approximately Draco constellation) and l

= 250°.3, b = -24°.6 (between Columba and Puppy constellations) respectively in a Galactic coordinate reference system, as shown in figure 1.4.

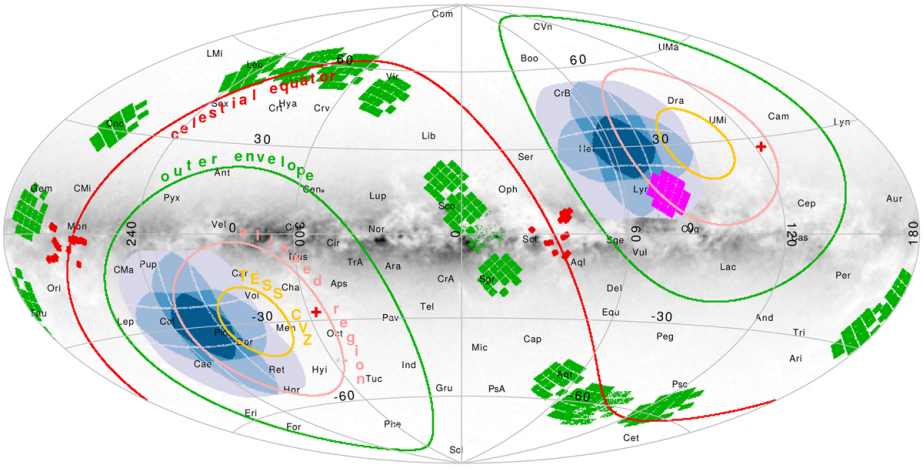

Figure 1.3: All-sky Aitoff projection in Galactic coordinates depicting the provisional pointing of PLATO's northern (LOPN1) and southern (LOPS1) long-duration phase fields: the pink circles represent the allowed regions for the LOP centers, the green circles the outer envelopes of every allowed field choice. The blue shades correspond to the previous PLATO provisional fields as reported in the Definition Study Report. The yellow, red, magenta and green plots indicate the TESS, Corot, Kepler and K2 fields.

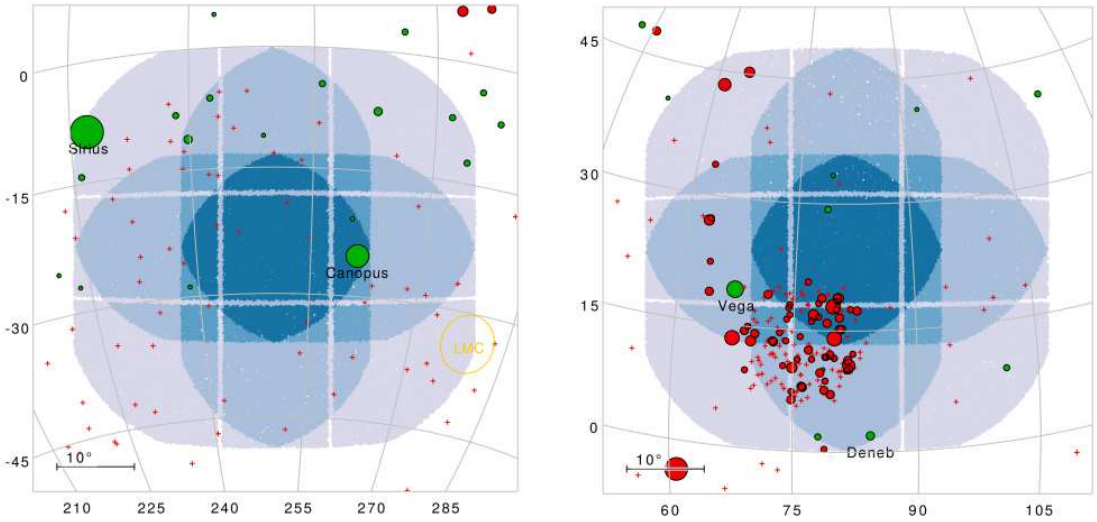

Figure 1.4: Location of the provisional PLATO LOPS1 (left) and LOPN1 (right) fields described in [5].

The PLATO Science Working Team has recently selected the first PLATO Long-duration

Observation phase (LOP) field, named LOPS2[12] and centered on l = 255°.9 and b = -24°.6, as can be seen in figure 1.5.

Indeed since the publication of the aforementioned paper, the position of the recommended LOP field in the Southern hemisphere has been moved to ensure that the selected field is independent of the initial spacecraft rotation angle after launch.

Moreover LOPS2 has been chosen as the first observation field because the ground-based facilities available in the Southern hemisphere can provide the best capabilities for the mass determination of the Earth-size planets discovered by PLATO in the habitable zone of Sun like stars.

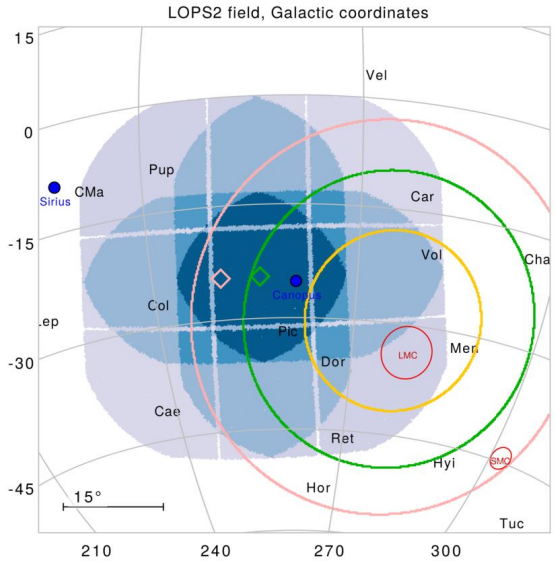

Figure 1.5: Location of the current LOPS2 field.

1.2.2 Stellar samples

Gaia mission is and will continue to be instrumental to identify bright, nearby cool F-, G-, K-, M-dwarfs and sub-giants across the huge sky region covered by the PLATO fields. In order to achieve the science requirements, five stellar samples have been defined for the PLATO observations. The first one (P1) is considered the highest priority objective for the mission and includes the "Rosetta stone targets" for PLATO, i.e. those sources with the highest

[12]The announcement of the first observation field can be seen at `https://www.cosmos.esa.int/web/plato/first-sky-field`

likelihood to fulfill the ultimate goal to compute a catalogue of highly accurately characterised long-period small planets in the habitable zone of solar-like stars. These stars have a spectral type from F5 to K7, which corresponds, for solar metallicity and Main Sequence phase, to the mass interval 0.6 - 1.4$M\odot$.
The fourth stellar sample is instead specifically directed to a survey of cool late type dwarfs in the solar vicinity.

In table 1.1 the constraints applied on the number of sources, the spectral type, the luminosity class, the magnitude range and the random photonic noise are reported for each stellar sample. In particular, a value of the random noise of 50 ppm in one hour allows to reduce the number of spurious detections: indeed 100% of the transits of Earth-sized planets in front of a solar-like star can be detected, while the detection rate decreases to 50% with an accuracy of 80 ppm in one hour.

	P1	P2	P4	P5	Colour sample
Stars	$\geq$ 15000	$\geq$ 1000	$\geq$ 5000	$\geq$ 245000	300
Spectral type	F5 - K7	F5 - K7	M	F5 - late K	anywhere in HRD
Limit V	11	8.5	16	13	-
NSR (ppm in 1h)	50	50	800	-	-
Wavelength (nm)	500 - 1000	500 - 1000	500 - 1000	500 - 1000	500 - 675, 675 - 1000
Observation phase	LOP	LOP	LOP	LOP	SOP

Table 1.1: Science requirements for PLATO stellar samples

PLATO samples considered in the asPIC include an FGK dwarf and subgiant sample of 2 378 177 stars with $V \leq 13, logg > 3.5$, 3870 K $< Teff <$ 6510 K and median distance = 428 pc, and an M dwarf sample of 297 362 stars with $V \leq 16, logg > 3.5$, $Teff \leq$ 3870 K and median distance = 146 pc. These sources have been selected accordingly to the criteria listed in table 1.2 in order to include only the required spectral classes and avoid contaminants as distant massive bright dwarfs and subgiants of spectral type earlier than F5 independently of their reddening.

FGK sample	M sample
$0.56 \leq (G_{BP} - G_{RP})_0 < 1.84$	$(G_{BP} - G_{RP})_0 \geq 1.84$
$M_{G,0} \leq 4.1(G_{BP} - G_{RP})_0 + 5.0$	$M_{G,0} > 2.334(G_{BP} - G_{RP})_0 + 2.259$
$M_{G,0} \geq 4.1(G_{BP} - G_{RP})_0 - 2.2$	Distance < 600 pc

Table 1.2: Selection criteria for PLATO stellar samples in asPIC1.1.
G, G_{BP}, G_{RP} are the Gaia apparent magnitudes, $M_{G,0}$ the Gaia intrinsic absolute magnitude and V the apparent visual magnitude.

In particular, the PLATO Input Catalogue for LOPS2 contains more than 9000 dwarf and subgiant stars of spectral types from F5 to K7 with $V < 11$ that will be observed with a random noise lower than 50 ppm in one hour, and more than 159 000 dwarf and subgiant stars of spectral types from F5 to K7 with $V < 13$.

1.2.3 Target characterization and follow-up

From available galactic absorption maps the reddening results to be negligible up to 70 pc from the Sun, it remains very low up to 400 pc and rapidly increases just before 1 kpc. F-type stars, being intrinsically more luminous, are located at larger distances on average than later type stars, and are therefore the most affected by reddening; nevertheless, at the limiting magnitude V = 11, the brightest F5 stars of sample P1 can be observed out to 300 pc and are therefore not likely to be much extincted or polluted.

Other than extinction, each PIC target has been characterized via cross-matching catalogues with a set of astrophysical parameters such as distance, proper motion, magnitudes, T_{eff}, surface gravity, metallicity [M/H] and age indicators; moreover, the considered samples include stars with different magnetic activity levels, in order to investigate the properties of planetary systems in an evolutionary contest. Stellar activity in particular can be a limiting factor for planet detection and mass measurements and also directly impact the planet's habitability.

The ground-based follow-up observations to be carried out by the GOP team are divided into two categories: the filtering observations are those designed to detect false positives,

while the radial velocity observations are those needed to characterise the planetary orbit. The former include low-precision and high-resolution spectroscopy, transit photometry, high-resolution imaging and Rossiter-McLaughlin (RM) observations; the latter require very high resolution in the spectroscopic measurements, indeed the typical photon-noise benchmarks for the ESPRESSO spectrograph on the Very Large Telescope (VLT) at Cerro Paranal (8.2m diameter telescopes) are 10 cm/s in 15 min for a V = 8 star.

Chapter 2

Gaia space mission

2.1 Mission overview

Gaia, labelled "ESA's billion star surveyor", is an exceptionally complex space observatory from the European Space Agency and constitutes a cornerstone mission for its unprecedented range and accuracy.

The primary scientific goal of Gaia is to clarify the origin and history of the Milky Way by examining its kinematical, dynamical, and chemical structure and evolution.
Indeed, as stated in Perrymn et al. 2001 [6], *"understanding the details of the Galaxy in which we live is one of the great intellectual challenges embraced by modern science"*.

For this purpose the mission aims to create an extraordinarily precise three-dimensional map of about one billion stars throughout the Galaxy from a quantitative census of the stellar populations, involving the measurements of their positions, distances and space motions and the determination of their astrophysical properties, such as surface gravity and effective temperature (Gaia Collaboration et al. 2016 [7]).
In addition, the data of Gaia will have a strong impact on many other areas of astrophysical research, including stellar evolution and physics, star formation, stellar variability, the distance scale, multiple stars, exoplanets, solar system bodies, unresolved galaxies and quasars, and fundamental physics.

The science data of Gaia comprise absolute astrometry (positions, proper motions, and parallaxes with an accuracy of 7 μas at G = 10 mag and 26 μas at G = 15 mag), broad-band G photometry down to 20 mag, low-resolution blue and red (spectro-)photometry (BP/RP spectra) and integrated G_{BP} and G_{RP} photometry for all objects, while medium-resolution spectroscopic data (RVS spectra) are collected for the brightest few hundred million sources with accuracies of 1–15 km s^{-1} down to 16.2 mag.

Gaia's telescopes and detectors can detect stars up to 400 000 times fainter than those visible to the naked eye[1]. For objects 4000 times fainter than the naked eye limit (that is, brighter than 15 magnitudes), Gaia is measuring their positions to an accuracy of 24 microarcseconds, comparable to measuring the diameter of a human hair at a distance of 1000 km.

Not only is Gaia a powerful all-sky, high spatial resolution, high astrometric and photometric accuracy survey, but also it is the biggest spectroscopic survey of its kind and the most cited astrophysics space mission to date.

The Gaia collaboration has been honored with the 2023 Berkeley prize for Meritorious Work in Astronomy "for enabling a transformative, multidimensional map of the Milky Way"[2]. According to the prize statement, *"Gaia's three data releases will long be regarded as major events in the history of astronomy, triggering a global partnership to better understand the origin, structure, and destiny of our home galaxy. [...] Gaia will forever remain a landmark achievement in humanity's story of cosmic exploration."*

[1]The limiting magnitude for naked eye visibility refers to the faintest stars that can be seen with the unaided eye, and in exceptionally good conditions amounts to about 6.5 mag. Gaia is able to observe stars down to 20.7 magnitudes.

[2]See `https://aas.org/grants-and-prizes/lancelot-m-berkeley-new-york-community-trust-prize-\meritorious-work-astronomy`.

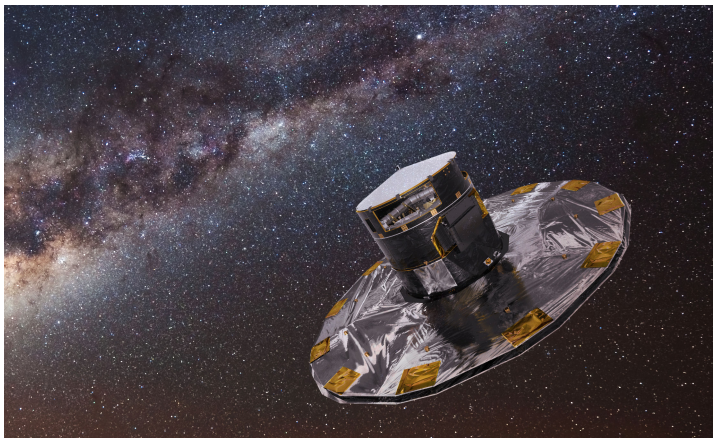

Figure 2.1: Gaia visualization.
Credits: ESA

2.1.1 Mission design

Gaia was launched on 19 December 2013 on a Soyuz vehicle from Europe's Spaceport in French Guiana and arrived at its operating point, the second Lagrange point of the Sun-Earth-Moon system, a few weeks later. The mission started with four weeks of special, ecliptic-pole scanning and subsequently transferred into its full-sky nominal scanning mode from its controlled Lissajous-type orbit around L2.

Gaia's revolving scanning law, which describes the intended spacecraft pointing as a function of time, is one of the keys to the astrometric performance of the mission.

It is worth mentioning that the number of observations is systematically higher especially at the poles and at ecliptic latitudes $|\beta| = \pm 45°$ due to the spacecraft's solar aspect angle and that the Ecliptic Pole Scanning Law (EPSL) is more prone to aliasing with respect to the Nominal Scanning Law (NSL), the latter having a sparser and more randomized sampling (Eyer at al. 2017 [8]).

To cover the whole sky, the satellite continuously spins around its axis, making four full rotations per day with a constant speed of 60 arcsec s^{-1}. Over a period of 6 hours, Gaia's two astrometric fields of view separated by the basic angle of 106.5 ° scan across all objects located along the great circle perpendicular to the spin axis, and as it slowly precesses around the solar direction with a constant aspect angle of 45 °, different parts of the sky are covered.

Over the course of the nominal operational lifetime each star has been observed an average of 70 times. The nominal five-year mission was supposed to end in July 2019, but it has been extended thrice; in March 2023, the continuation of the operations for Gaia mission has been confirmed through the second quarter of 2025, with a post-operations phase that will be completed by 31 December 2030.

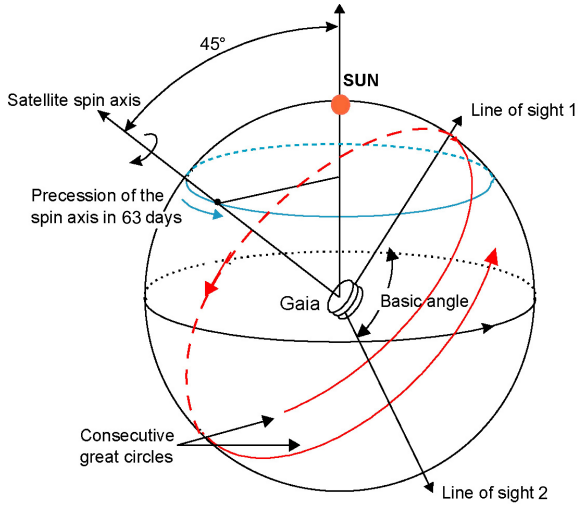

Figure 2.2: Gaia's scanning law

Gaia's telemetry is transmitted by low-gain antenna to the mission's ground stations, which deliver it to the Mission Operation Centre (MOC), located at ESA ESOC in Darmstadt, Germany. All the science operations are carried out at ESA ESAC in Madrid, Spain, where the data provided by the MOC undergoes a preliminary processing phase; from ESAC it is then distributed to six Data Processing Centres (DPCs) across Europe, that together constitute the Data Processing and Analysis Consortium.

2.1.2 Instrumentation and payload

Gaia's payload module houses two identical telescopes for the purpose of performing global astrometry, which share a common focal plane along with the astrometric, photometric and spectroscopic instruments. The focal plane assembly features 106 charge-coupled-device (CCD) detectors, for a total of nearly one billion pixels (a 'gigapixel') and is the largest focal plane ever flown in space. Three types of CCDs can be distingushed on the basis

of their bandpasses and functionalities: broad-band (for metrology, sky mapping, astrometry, photometry), blue-enhanced and red-enhanced (for photometry, low-resolution spectrophotometry and medium resolution spectroscopy).

The astrometric instrument measures stellar positions on the sky, in order to deduce their parallax and thus their distance, as well as the velocity of the stars as they move across the plane of the sky. The bandpass of the astrometric field detectors, defining the Gaia G band, covers 330-1050 nm.

The photometric instrument provides colour information for celestial objects and consists of two fused-silica prisms, known as the blue (BP) and the red (RP) photometer, whose passbands are respectively of 330-680 nm and 630-1050 nm.

Gaia's spectroscopic instrument is the Radial-Velocity Spectrometer (RVS), an integral-field spectrograph with resolving power R = 11 500 which covers the wavelength range 845-872 nm. RVS reveals the velocity of the star along the line of sight by measuring the Doppler shift of the absorption lines.

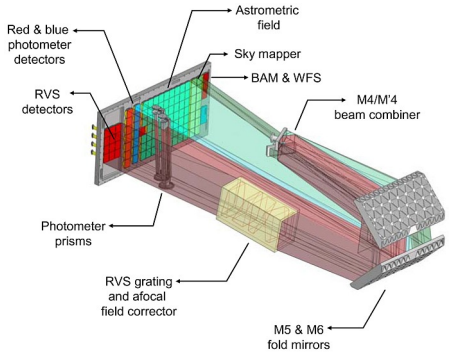

Figure 2.3: Gaia's scientific instrumentation.

2.1.3 Scientific objectives and achievements

Gaia's survey of stars across the entire sky, down to extremely faint limits with a level of precision never accomplished before, provides measurements of stellar distances and motions for large samples of stars of different masses, ages and compositions. This will enable the discovery of families of stars that share peculiar motions around the Galaxy or anomalous compositions, which could be the remnants of a once-separate galaxy that the Milky Way

has consumed.

The Gaia results will clarify the origin and formation history of our Galaxy, precisely identify relics of tidally-disrupted accretion debris, probe the distribution of dark matter and establish the luminosity function for pre-main sequence stars. They will also help to detect and categorize rapid evolutionary stellar phases, placing unprecedented constraints on the age, internal structure and evolution of all stellar types.

Moreover, Gaia will measure the deflection of starlight due to the gravitational fields of individual objects in the Solar System, will investigate Trojan asteroids around Jupiter, Venus, Mars and Earth and the origin of comet showers. Gaia is expected to find at least 2000 extra-solar planets from photometric transits and astrometric measurements[3], identify tens of thousands of brown dwarfs and white dwarfs, and discover thousands of extragalactic supernovae.

Among Gaia's many scientific discoveries and achievements so far, we recall the following:

- In May 2016 Gaia detected its first superluminous supernova[4].
- Gaia may have found the missing link in black hole evolution[5]: an intermediate-mass black hole in the ancient globular cluster Messier 4.
- A new map of part of the Milky Way has been realized, based on the combination of several different Gaia data sets such as YSO groups, Cepheids, High-Mass Star Forming Regions, OB stars, Young Open Clusters and 3D dust [6].
- Gaia's photometric observations have allowed the mission's very first detection of two extra-solar planets, named Gaia-1b and Gaia-2b and announced in May 2022[7].

[3]The fourth data release, which is expected to be published no sooner than in the end of 2025, will include a detailed and updated exoplanet list.

[4]For reference: `https://doi.org/10.48550/arXiv.1611.10207`.

[5]See `https://doi.org/10.1093/mnras/stad1068`.

[6]Credits to the "Mapping the Milky Way: Galactic Cartography in the Age of High Precision Parallaxes" workshop (`https://www.lorentzcenter.nl/mapping-the-milky-way.html`).

[7]See `https://doi.org/10.48550/arXiv.2205.10197`.

- Astrometric data from Gaia allowed astronomers to discover and then directly image a giant exoplanet using Japan's Subaru Telescope [8].
- First confirmed discovery of a black hole with Gaia data, referred to as Gaia BH1. Located at 480pc from the Sun, it is also the nearest black hole ever found[9].
- First ever recorded stellar occultation by the Near Earth asteroid Didymos[10].
- The observation of asymmetrical tidal tails of open star clusters challenges Newtonian gravitation in favour of MOND theory[11].
- Gaia's RSV spectra allowed to obtain the first homogeneous all-sky survey of the Diffused Interstellar Bands (DIB) in the Interstellar Medium.
- Gaia revealed the chemical signature of the Galactic spiral arms[12].

2.2 Gaia Data Release 3

The Gaia Data Release 3 (Gaia DR3) catalogue has been released on 13 June 2022 and is the outcome of the processing of raw data collected with the Gaia instruments during the first 34 months of the mission[13] by the Gaia Data Processing and Analysis Consortium (Gaia Collaboration et al. 2022 [9]).

Counting almost two billions sources (precisely 1 811 709 771 objects), this is is the largest collection to date of all-sky astrometry, spectrophotometry, radial velocities, variables, and astrophysical parameters.

It contains the same source list, celestial positions, proper motions, parallaxes, and broad band photometry already present in the Early Third Data Release, Gaia EDR3 (meaning full astrometry for 1 467 744 818 sources, G magnitudes for around 1.806 billion sources, G_{BP}

[8] See `https://www.science.org/doi/10.1126/science.abo6192`.
[9] See `https://arxiv.org/abs/2209.06833andhttps://www.mpia.de/news/science/2022-16-gaia-bh1`.
[10] Further details can be found at `https://lagrange.oca.eu/fr/results`.
[11] See `https://arxiv.org/abs/2210.13472`.
[12] See `https://arxiv.org/abs/2206.14849`.
[13] Gaia DR3 is based on data collected between 25 July 2014 (10:30 UTC) and 28 May 2017 (08:44 UTC), with J2016.0 as reference epoch in Julian Days.

and G_{RP} magnitudes for around 1.54 billion and 1.55 billion sources).

Additionally, the Gaia DR3 catalogue includes about 1 million RVS mean spectra and radial velocities for 33 812 183 sources from the radial velocity spectrometer, about 220 million low-resolution XP mean spectra[14], photometric time series for 10.5 million variable sources and for 1.2 million sources from the Gaia Andromeda Photometric Survey (GAPS), radial velocity time series for 1898 Cepheids and RR Lyrae stars, 5 all-sky total galactic extinction maps, astrophysical parameters (such as T_{eff}, log(g), [M/H], A_G, distance, etc.) for 475 million objects, 158 152 Solar-system objects (including near-Earth and main-belt asteroids and trans-Neptunian objects), 813 687 non-single stars (binary and multiple star systems), 6 649 162 QSO candidates and 4 842 342 galaxy candidates.

The time coordinate for Gaia DR3 results is the Barycentric Coordinate Time (TCB): the epoch photometry times are measured in Barycentric Julian Days (BJD) in units of TCB with an offset of JD 2455197.5, following the time coordinate convention used in the Gaia Archive.

The G-band photometric uncertainties are ≈0.3 mmag for $G < 13$, 1 mmag at G=17, and 6 mmag at G=20 mag. The G_{BP}-band photometric uncertainties are ≈0.9 mmag for $G < 13$, 12 mmag at G=17, and 108 mmag at G=20 mag. The G_{RP}-band photometric uncertainties are ≈0.6 mmag for $G < 13$, 6 mmag at G=17, and 52 mmag at G=20 mag.

2.2.1 Variability

Investigating time variability of astronomical objects begins with detecting any significant changes in their brightness. Gaia is an exceptional survey for variability analysis, indeed it offers the unique opportunity to study variability of close to 2 billion objects: its wide-range multi-epoch and quasi-simultaneous photometric observations and its irregular sparse sampling allow for the detection of periodic signals ranging from minutes to years and for medium to long-term non-periodic variability (Eyer at al. 2022 [10]).

As stated in Rimoldini at al. 2022 [11], time-dependent brightness variations of celestial

[14]Also called BP/RP mean spectra, which are the BP + RP externally calibrated combined mean spectra, sampled on a predefined wavelength grid from 336 nm to 1020 nm with a step of 2 nm.

objects may be caused by different phenomena, and a certain set of classes can be identified to describe different variability types. Moreover, the presence of radial velocity variations means, for a pulsating star, that the radius of the source is physically changing with time; if the pulsations are strictly periodic, the radial velocity curve will be as well.
Thanks to the extensive cross-match of Gaia sources compiled by Gavras et al. 2023 [12], which provided millions of variable objects from the literature, in total 10.5 million sources in GDR3 (between 9.5 million variable stars and 1 million Active Galactic Nuclei/Quasars, all provided with epoch photometry) have been classified into 24 variability types of periodic and non-periodic variables (pulsating, eclipsing, rotating, eruptive, cataclysmic, stochastic, microlensing), with amplitudes from a few mmag to several magnitudes as can be seen in Table 2.1.

In addition, Gaia processing pipeline identified 2.5 million galaxies thanks to spurious variability, since they appear to be photometrically variable as a result of scan angle orientation effects induced by asymmetric extended sources.

Class name	Description
AGN	Active Galactic Nuclei (including Quasars).
$DSCT\|GDOR\|SXPHE$	Set of variable types: δ Scuti, γ Doradus and SX Phoenicis.
WD	White Dwarf variable stars of types: ZZ Ceti, V777 Herculis and GW Virginis.
LPV	Long Period Variable stars of types: o Ceti (Mira), OGLE Small Amplitude Red Giants, and semiregular.
$ACV\|CP\|MCP\|ROAM\|ROAP\|SXARI$	Set of variable types: α^2 Canum Venaticorum, Chemical Peculiar, Rapidly Oscillating and SX Arietis star.
S	Set of stars with short timescale variability.
MICROLENSING	Star with microlensing event.
CEP	Cepheid variable types: δ Cepheid, anomalous Cepheid, and type-II Cepheid.
YSO	Young Stellar Object.
RS	RS Canum Venaticorum type variable.
ACYG	α Cygni-type variable.
BCEP	β Cephei type variable.
$BE\|GCAS\|SDOR\|WR$	Subset of eruptive variable types: B-type emission line star, Γ Cassiopeiae, S Doradus, and Wolf-Rayet.
SN	Supernovae.
SPB	Slowly Pulsating B-star variable.
ECL	Eclipsing Binaries of types: β Persei (Algol), β Lyrae, and W Ursae Majoris.
ELL	Ellipsoidal variable.
SYS	Symbiotic variable star.
SOLAR LIKE	Stars with solar-like variability due to flares, spots, and rotational modulation.
CV	Cataclysmic variable
SDB	Sub-dwarf B stars of types: V1093 Her and V361 Hya.
RR	RR Lyrae stars of the following types: fundamental mode, first-overtone, double mode and anomalous mode.
EP	Star with exoplanet transits.
RCB	R Coronae Borealis type variable.

Table 2.1: Variability classes identified in Gaia DR3.

Moreover, tailored analyses called Specific Object Studies (SOS) processing packages have been performed for 11 variability types, whose detailed results are provided in separate tables accessible from the Gaia Archive.

The variable classes identified by the SOS modules have been reported in table 2.2.

SOS type	Sources
Cepheids	15 021
Compact companions	6306
Eclipsing binaries	2 184 477
Long-period variables	1 720 588
Microlensing events	363
Planetary transits	214
RR Lyrae stars	271 779
Short-timescale variables	471 679
Solar-like rotational modulation variables	474 026
Upper-main-sequence oscillators	54 476
Active galactic nuclei	872 228

Table 2.2: Specific Object Studies modules in GDR3.

Chapter 3

Variability analysis

3.1 Preliminary work

Variability analysis can be defined as the comprehensive assessment of the degree and character of patterns of variation of the source's brightness over time intervals.
Variable stars can be intrinsic (such as pulsating and eruptive stars) or extrinsic (as in the case of eclipsing binaries and rotating spotted stars). As already stated in the Introduction to the present work, a detailed knowledge of the (solar-type) host star, its flux variability in time and its surroundings is required in order to detect extra-solar planets. For instance, most planet confirmation relies on the Doppler wobble of the host star, induced by the planet. Moreover, we can learn about a planet's dynamical history from mapping its projected orbit as it transits its host star. Hence, stellar surface inhomogeneities can impact planetary interpretations, and can completely swamp the signals from terrestrial worlds. Stellar activity in particular can be a limiting factor for planet detection and mass measurements and also directly impact the planet's habitability.
Conversely, a background binary star blended in the same pixels as the bright target star inside PLATO's PSF would produce a diluted transit in the target star's lightcurve, comparable to that of a planet, thus mimicking a planetary transit signature.

In this thesis work I analyzed two samples of stars obtained from the two outer regions

enveloping the provisional Long-duration Observation Phase (LOP) north and south fields in the PLATO Input Catalogue, selected as explained in [5] and in section 1.2.1.
The considered sources, selected from Gaia Data Release 3, are spread over two conical regions of 52°radius, with ecliptic latitude $|\beta| > 38°$ to allow for a proper orientation of the spacecraft and envelope every possible field choice. These two outer caps count respectively 543 394 and 593 563 targets, that in this work have been cross-matched by the unique source identifier *source_id* with each variable source of the 11 Specific Object Studies (SOS) modules in Gaia Data Release 3.
As described in [10] and section 2, these variability classes include RR Lyrae stars, Cepheids, eclipsing binaries, upper Main Sequence oscillators, solar-like variables with rotational modulation, short timescale variables, long period variables, active galactic nuclei, microlensing events, compact companions and stellar hosts of transiting extra-solar planets.

The outcome of this cross-matching operation is the distribution of several classes of variable objects in the all-sky PLATO Input Catalogue that is reported in table 3.1.

Variability class	LOPN1	LOPS2	Total
Short timescale	2996	4081	7077
Eclipsing binaries	2977	3467	6444
Solar-like	1794	1849	3643
MS oscillators	153	438	591
RR Lyrae	84	78	162
Exoplanetary hosts	21	31	52
Cepheids	1	0	1
Long period	0	1	1

Table 3.1: Variable sources in the PIC outer LOP fields.

No Active Galactic Nuclei, microlensing events and compact companions from Gaia DR3 resulted to be collected in the PLATO Input Catalogue.

The resulting non-null variability classes have been complemented with selected photometric, spectroscopic, astrometric and astrophysical parameters of the sources, obtained via ADQL (Astronomical Data Query Language) Advanced Search in the Gaia Archive[1] query

[1] `https://archives.esac.esa.int/gaia`

interface.

Non tabular data such as epoch photometry in the G, G_{BP} , and G_{RP} bands have instead been extracted via DataLink from the Gaia Archive.

The main parameters selected for each of the aforementioned classes of variable objects have been collected in Tables 3.2a and 3.2b.

The all-sky distribution of the different classes of variable sources in Aitoff projection and Galactic coordinates is displayed in Figure 3.1, while the absolute Color-Magnitude Diagrams (reddened and corrected for extinction) are shown in figure 3.2.

For each variability class, sky map distributions, observational Hertzsprung–Russell diagrams and photometric time series have been obtained.

Moreover in order to characterize variability the statistics of photometric time series have been exploited, such as the Abbe value and the skewness magnitude for G FoV transits, that together constitude a metric targeting non-periodic variations.

The Abbe value, or von-Neumann ratio statistic, measures the point-to-point scatter in a photometric time series, and is an estimate of the regularity of the light curve variability pattern over the duration of the observations; in other words it estimates the smoothness of the light curve. It has a value of about one for purely noisy time series of a constant function, and decreases to zero for time series displaying a smooth pattern of variability between successive measurements (N. Mowlavi 2014 [13]). The skewness of the magnitude distribution is instead given by the ratio of the phase duration of the descending branch to the rising branch and is a measure of the asymmetry of the light curve. For a pure sinusoidal or symmetric curve this value is unity (Bellinger et al. 2019 [14]).

A metric targeting periodic variations is given by the distribution of the ratio of the two bands mean photometric uncertainties as a function of the median magnitude in the G band, where stellar pulsations are expected to exhibit larger variations in the G_{BP} than in the G_{RP} band[2]. The ratio is instead close to one for non-pulsating objects, apart from the increasing

[2]Further details concerning the inverse dependence between light amplitude variation and wavelength for pulsating stars may be found in R. Townsend 2002 [15]

scatter towards faint magnitudes due to shot noise [11].

In the following sections the main properties of the variable sources located in the northern and southern outer LOP fields are investigated. For the sake of readability, from now on the outer regions (ecliptic caps with $|\beta| > 38°$) hosting the PLATO Input Catalogue sources analyzed in this work will be referred to as LOPN1 and LOPS2.

	Variability types			
gaiadr3. tables	**RR Lyrae**	**Cepheids**	**planetary transits**	**eclipsing binaries**
gaia_source	l	l	l	l
gaia_source	b	b	b	b
gaia_source	parallax	parallax	parallax	parallax
gaia_source	ag_gspphot	ag_gspphot	ag_gspphot	ag_gspphot
gaia_source	ebpminrp_gspphot	ebpminrp_gspphot	ebpminrp_gspphot	ebpminrp_gspphot
vari_summary	median_mag_g_fov	median_mag_g_fov	median_mag_g_fov	median_mag_g_fov
vari_summary	median_mag_bp	median_mag_bp	median_mag_bp	median_mag_bp
vari_summary	median_mag_rp	median_mag_rp	median_mag_rp	median_mag_rp
vari_summary	skewness_mag_g_fov	skewness_mag_g_fov	skewness_mag_g_fov	skewness_mag_g_fov
vari_summary	abbe_mag_g_fov	abbe_mag_g_fov	abbe_mag_g_fov	abbe_mag_g_fov
vari_summary	std_dev_mag_bp	std_dev_mag_bp	std_dev_mag_bp	std_dev_mag_bp
vari_summary	std_dev_mag_rp	std_dev_mag_rp	std_dev_mag_rp	std_dev_mag_rp
vari_type	source_id	source_id	source_id	source_id
vari_type	p_f	p_f	transit_period	frequency
vari_type	p1_o	p1_o		
vari_type	peak_to_peak_g			
vari_type	metallicity			
vari_type	best_classification	type_best_classification		
vari_type	reference_time_g	reference_time_g	transit_reference_time	reference_time
vari_type	reference_time_bp	reference_time_bp		
vari_type	reference_time_rp	reference_time_rp		
vari_type	reference_time_rv			
datalink	G, BP, RP time series	G, BP, RP time series	G, BP, RP time series	G, BP, RP time series
vari_epoch_radial_velocity	rv_obs_time			
vari_epoch_radial_velocity	radial_velocity			
vari_epoch_radial_velocity	radial_velocity_error			

(a)

	Variability types			
gaiadr3. tables	**rotation modulation**	**MS oscillator**	**short timescale**	**long period**
gaia_source	l	l	l	l
gaia_source	b	b	b	b
gaia_source	parallax	parallax	parallax	parallax
gaia_source	ag_gspphot	ag_gspphot	ag_gspphot	ag_gspphot
gaia_source	ebpminrp_gspphot	ebpminrp_gspphot	ebpminrp_gspphot	ebpminrp_gspphot
vari_summary	median_mag_g_fov	median_mag_g_fov	median_mag_g_fov	median_mag_g_fov
vari_summary	median_mag_bp	median_mag_bp	median_mag_bp	median_mag_bp
vari_summary	median_mag_rp	median_mag_rp	median_mag_rp	median_mag_rp
vari_summary	skewness_mag_g_fov	skewness_mag_g_fov	skewness_mag_g_fov	skewness_mag_g_fov
vari_summary	abbe_mag_g_fov	abbe_mag_g_fov	abbe_mag_g_fov	abbe_mag_g_fov
vari_summary	std_dev_mag_bp	std_dev_mag_bp	std_dev_mag_bp	std_dev_mag_bp
vari_summary	std_dev_mag_rp	std_dev_mag_rp	std_dev_mag_rp	std_dev_mag_rp
astrophysical_parameters		mg_gspphot		
astrophysical_parameters		vsini_esphs		
vari_type	source_id	source_id	source_id	source_id
vari_type	best_rotation_period	frequency1	frequency	frequency
vari_type	max_activity_index_g	amplitude_g_freq1	amplitude_estimate	amplitude
vari_type	segments_rotation_period			
vari_type	segments_start_time			
vari_type	segments_end_time			
datalink	G, BP, RP time series	G, BP, RP time series	G, BP, RP time series	G, BP, RP time series

(b)

Table 3.2: Astrometric, photometric, spectroscopic and astrophysical parameters for each GDR3 variability class SOS module in the PLATO Input Catalogue.

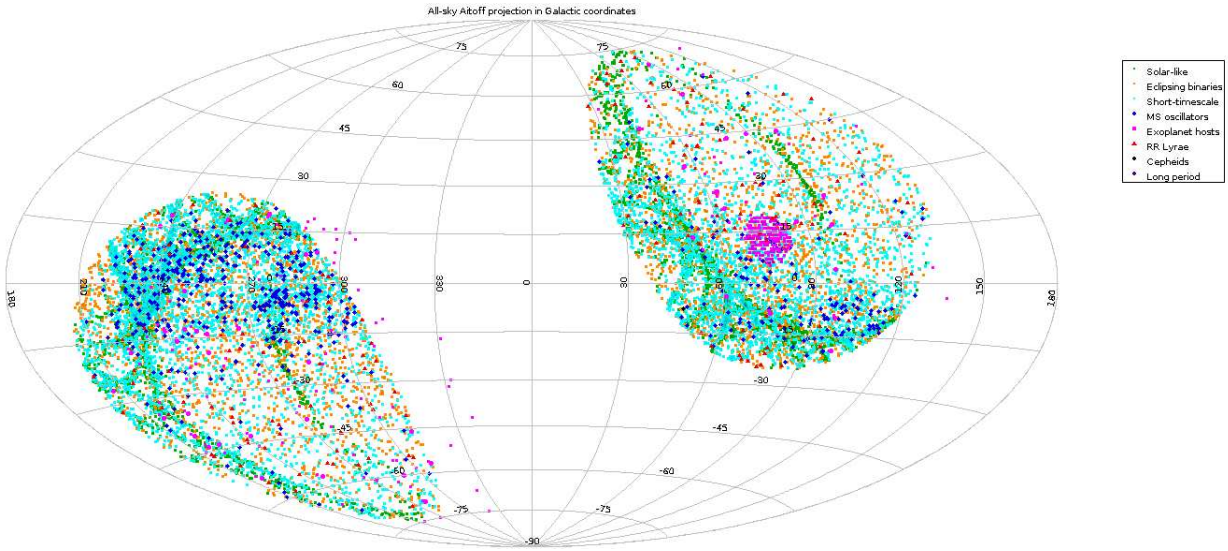

Figure 3.1: All-sky distribution of the variable sources in Aitoff projection and Galactic coordinates.

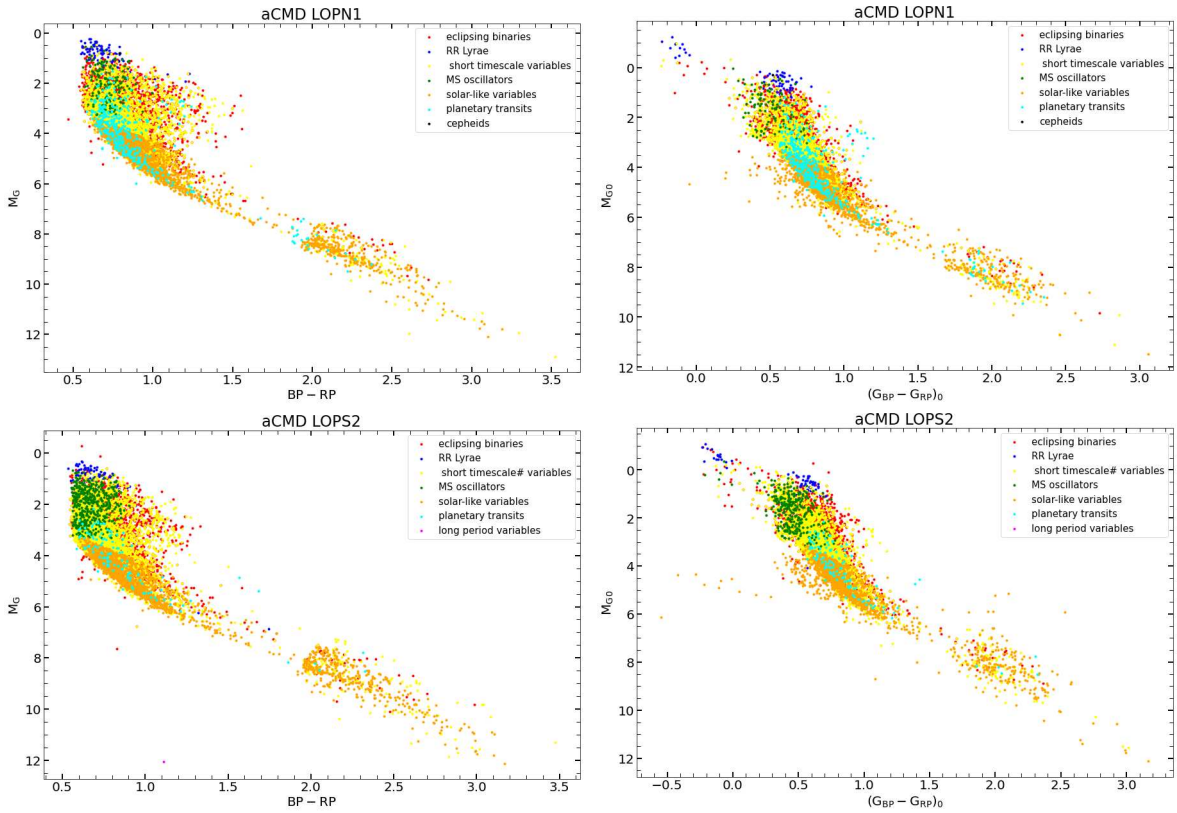

Figure 3.2: Top: absolute Color-Magnitude diagram (left) and extinction-corrected absolute CMD (right) for the northern outer field LOPN1. Bottom: same as above, but for LOPS2.

3.2 Planetary transits

This class of photometric variables includes Main Sequence FGK-type stars displaying signatures of exoplanetary transits. Thanks to the high spatial resolution and its multi-epoch photometry, and despite its sparse and low-cadence observations, Gaia can identify false-positive candidates and confirm true detections of transiting planets from TESS exoplanetary candidates. Indeed Panahi et al.[16] have confirmed the mission's very first two new Hot-Jupiters via RV follow up observations, Gaia-1b and Gaia-2b.

The Gaia DR3 planetary transits SOS module is composed of 173 known exoplanets with visible transits in the photometry of Gaia and 41 new candidates found by the mission's Data Processing and Analysis Consortium (DPAC); the sample has been obtained through a dedicated implementation of the BLS algorithm with the aim of searching for significant transit-like signals in the candidates light curves in the Full-Frame Image (FFI) photometry of TESS.

The known confirmed and the candidate transiting extra-solar planet hosts from Gaia DR3 that are included in the PLATO Input Catalogue are collected in tables 3.3 and 3.4 respectively for the two outer fields LOPN1 and LOPS2. Specifically 3 out of 21 are candidate exoplanetary hosts in the northern outer region, while 7 out of 31 are the candidates in the southern outer region.

We then procedeed to exploit the full list of all currently known confirmed planet hosts included in the asPIC1.1, available from the SSDC portal[3]. It consists of 859 stars of spectral class FGKM; after the imposition of the geometrical constraints $|\beta| > 38°$, the list is reduced to 403 planet hosts in the northern outer PLATO sky field LOPN1 and 92 planet hosts in the southern outer PLATO sky field LOPS2. Not surprisingly, most of the known northern field planets are actually Kepler objects since the Kepler Field is fully enveloped in LOPN1. For all the sources which did not have a match in the Gaia DR3 SOS module, we made use of the photometric and astrometric parameters collected in the PLATO Input Catalogue, as depicted in table 3.5.

[3]It can be retrieved as a .csv or .json file by selecting the flag for planet host from `https://tools.ssdc.asi.it/asPICtool/`.

Gaia DR3 *source_id*	Main ID	Spectral type	Exoplanet	References
1334573817793362560	HAT-P-18	K2V	HAT-P-18 b	4 5 6 7 8
1928431764627661440	BD+37 4734B	G0V	HAT-P-1 b	1 2 3 4 5
1962153854973972096	HAT-P-40	F	HAT-P-40 b	1 2 3 4 5
1316708918505350528	BD+28 2507	G1V	XO-1 b	1 2 3 4 5
1622997463177004928	WISEA J160752.17+574902.9		N/A	1 4 9
1864885215233116032	KELT-16	F7V	KELT-16 b	1 2 3 4 5
2262322556576778752	Qatar-10	F7V	Qatar-10 b	1 2 3 4 5
2244830490514284928	Qatar-1	K	Qatar-1 b	1 2 3 4 5
1424011082893734272	WASP-92	F7	WASP-92 b	1 2 3 4 5
4606030169272920320	HAT-P-5	G1V	HAT-P-5 b	1 2 3 4 5
2177849036734191744	TYC 3970-844-1		N/A	1 2 4 5
4609062308806929152	TYC 2620-648-1	F8	TrES-4 b	1 2 3 4 5
4609131509318715136	1SWASP J175207.01+373246.3	G	TrES-3 b	1 2 3 4 5
2102117871259036672	Kepler-7	G0	Kepler-7 b	1 2 3 4 5
2129256395211984000	BD+47 2846	F6V	HAT-P-7 b	1 2 3 4 5
2141754578242371584	WASP-48	G0IV	WASP-48 b	1 2 3 4 5
1499514786891168640	HAT-P-12	K5	HAT-P-12 b	1 2 3 4 5
4535127268607000320	WISEA J183411.49+220908.4		N/A	1 4 6
1644692064543192704	BD+66 911	K	KELT-23A b	1 2 3 4 5
1827242816201846144	HD 189733	K2V	HD 189733 b	1 2 3 4 5
1587399232335653760	WASP-113	G1	WASP-113 b	1 2 3 4 5

Table 3.3: List of the 21 confirmed and candidate transiting exoplanet hosts in LOPN1.

Gaia DR3 *source_id*	Main ID	Spectral type	Exoplanet	References
5345417757181174144	WISEA J114230.50-523738.6		N/A	1 4 6
5608644895310998272	HATS-51	G	HATS-51 b	1 2 3 4 5
5594445630358459648	2MASS J07545687-3221219		N/A	1 4 6
4895643593611507584	WISEA J041929.55-255735.4		N/A	1 4 6
4899428146994060800	HATS-5	K0	HATS-5 b	1 2 3 4 5
4906145613282734208	HATS-30	G1	HATS-30 b	1 2 3 4 5
4677436783705094912	WISEA J043143.94-612309.1		N/A	1 4 6
5565050255701441664	CD-38 3220	F6V	WASP-121 b	1 2 3 4 5
5583523425437258240	WASP-64	G7	WASP-64 b	1 2 3 4 5
5578530470116727936	WISEA J070548.04-351521.8		N/A	1 4 6
3211188618762023424	BD-06 1077	G0	WASP-35 b	1 2 3 4 5
5348534425968598400	TYC 8225-452-1		N/A	1 2 4 5
4851398799032507776	WASP-139	K0	WASP-139 b	1 2 3 4 5
4864759888238232320	WASP-159	F9	WASP-159 b	1 2 3 4 5
4955371367334610048	HD 10069	F6V	WASP-18 b	1 2 3 4 5
2959177048983750016	WASP-61	F7	WASP-61 b	1 2 3 4 5
5656896924435896832	HATS-26	F	HATS-26 b	1 2 3 4 5
5444147952811517696	WASP-66	F4	WASP-66 b	1 2 3 4 5
5557345496687437696	WASP-23	K1V	WASP-23 b	1 2 3 4 5
4746157737910069888	CD-50 714	F9	WASP-117 b	1 2 3 4 5
5086537022856406272	WASP-22	G	WASP-22 b	1 2 3 4 5
5089851638095503616	WASP-78	F8	WASP-78 b	1 2 3 4 5
6386751579018596864	WASP-91	K3	WASP-91 b	1 2 3 4 5
5735158757648658048	UCAC4 384-050987		N/A	1 2 4 5
5262709709389254528	TOI-150	F	TOI-150 b	1 2 3 4 5
5560886336446650240	CD-42 3043	G4	WASP-122 b	1 2 3 4 5
2980392087185289216	WASP-141	F9	WASP-141 b	1 2 3 4 5
5489780919480009472	CD-51 2720	G0	KELT-15 b	1 2 3 4 5
4911563216311083392	CD-56 324	G5	WASP-97 b	1 2 3 4 5
2991284369063612928	WASP-49	G6V	WASP-49 A b	1 2 3 4 5
5723772524469252096	WASP-169	G0	WASP-169 b	1 2 3 4 5

Table 3.4: List of the 31 confirmed and candidate transiting exoplanet hosts in LOPS2.

[4] `http://cdsportal.u-strasbg.fr/`

[5] `http://simbad.u-strasbg.fr/`

[6] `http://exoplanet.eu/catalog/`

[7] `https://vizier.cds.unistra.fr/`

[8] `https://exofop.ipac.caltech.edu/tess/`

[9] `https://ned.ipac.caltech.edu/`

Col. name	Description
sourceId	Gaia DR2 sourceId
ELAT	Ecliptic latitude of the object at the reference epoch
GLON	Galactic longitude of the object at the reference epoch
GLAT	Galactic latitude of the object at the reference epoch
BPRP	$(G_{BP} - G_{RP})$ colour
BPRP0	Dereddened $(G_{BP} - G_{RP})$ colour
BJgaiaMG0	Absolute intrinsic G magnitude
AG	Estimate of the extinction A_G in the G band
sourceFlag	Bitmask indicating if the source is a FGK or M star and if it hosts known planet(s)

Table 3.5: Description of the columns of the asPIC1.1 catalogue that we exploited in this work.

The sky distribution of all the PIC planetary transit events (whether alleged or confirmed) in Galactic coordinates and in Aitoff projection is shown in figure 3.3; their observational Hertzsprung-Russell diagrams are reported in figure 3.4.

Figure 3.6 displays the lightcurve of the confirmed exoplanetary host KELT-16 (Gaia DR3 *source_id* 1864885215233116032), a yellow-white star of spectral class F7V closely orbited by a hot Jupiter; in figure 3.7 instead the lightcurve of the candidate exoplanetary host TYC 3970-844-1 (Gaia DR3 *source_id* 2177849036734191744) is reported.

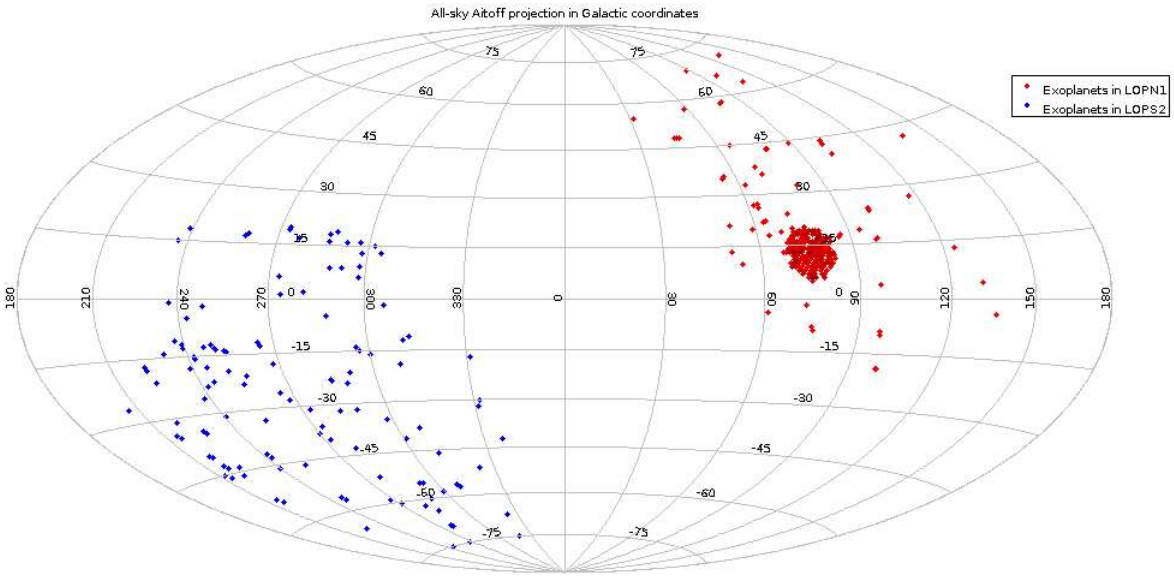

Figure 3.3: Sky map of the distribution of exoplanetary hosts in Galactic coordinates.

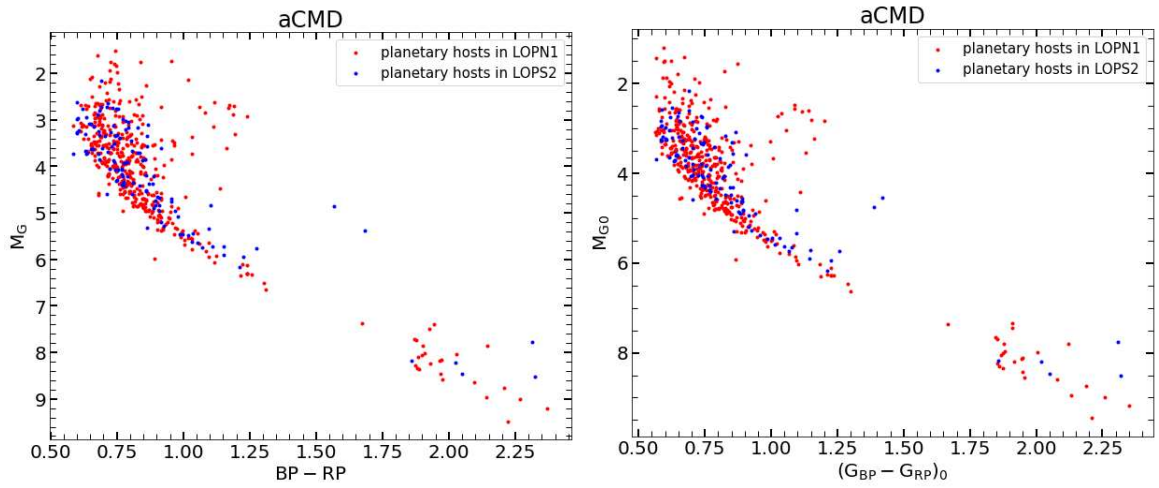

Figure 3.4: Absolute Color-Magnitude diagram (left) and extinction-corrected absolute CMD (right) for the total sample of planet hosts in PIC.

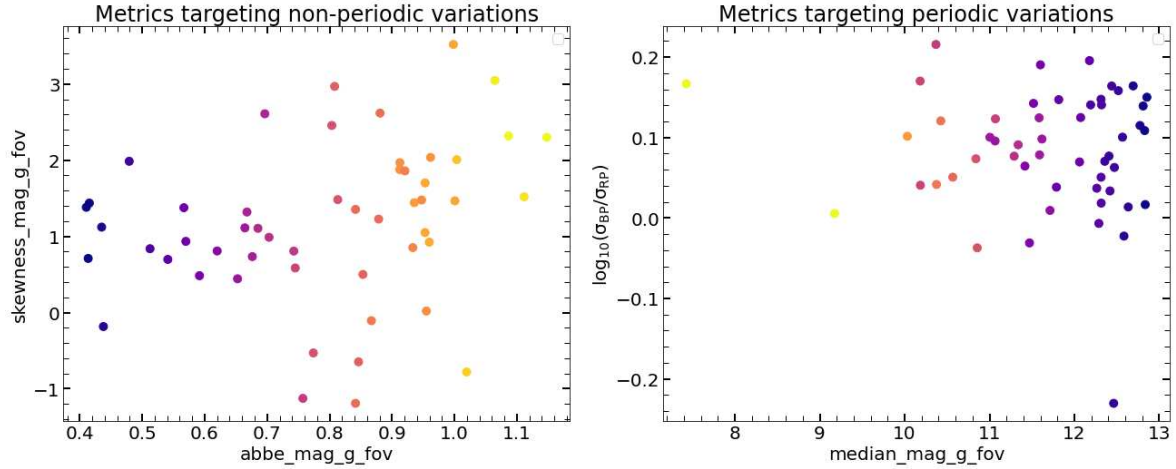

Figure 3.5: Metrics targeting non-periodic (left) and periodic (right) variations for planetary hosts.

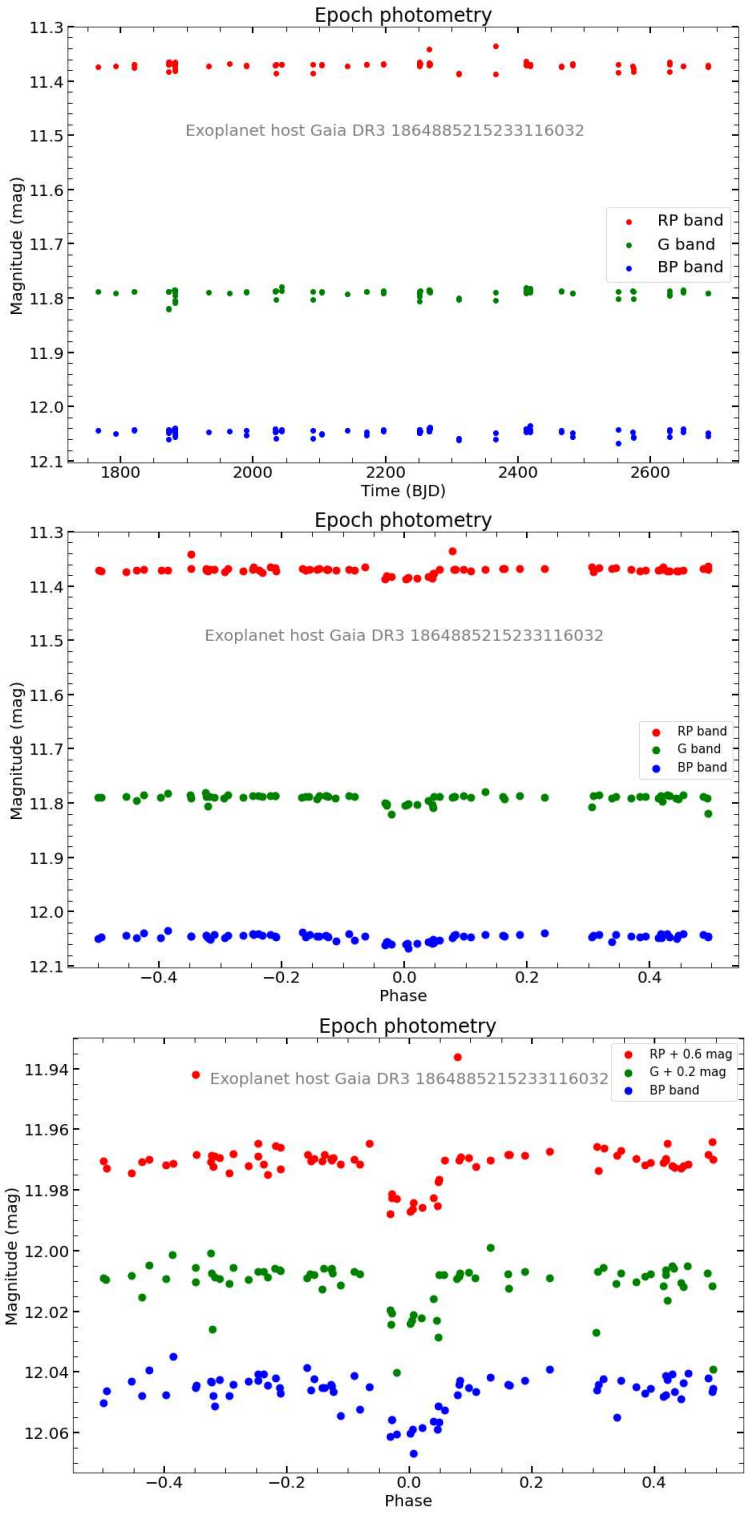

Figure 3.6: Top panel: full time-series in the G, G_{BP} and G_{RP} bands for the extra-solar planet host KELT-16 (Gaia DR3 1864885215233116032). Middle panel: phase-folded light curves according to the transit orbital period P = 0.97 d. Bottom panel: zoom on the phase diagram displaying the transit event in the three photometric bands.

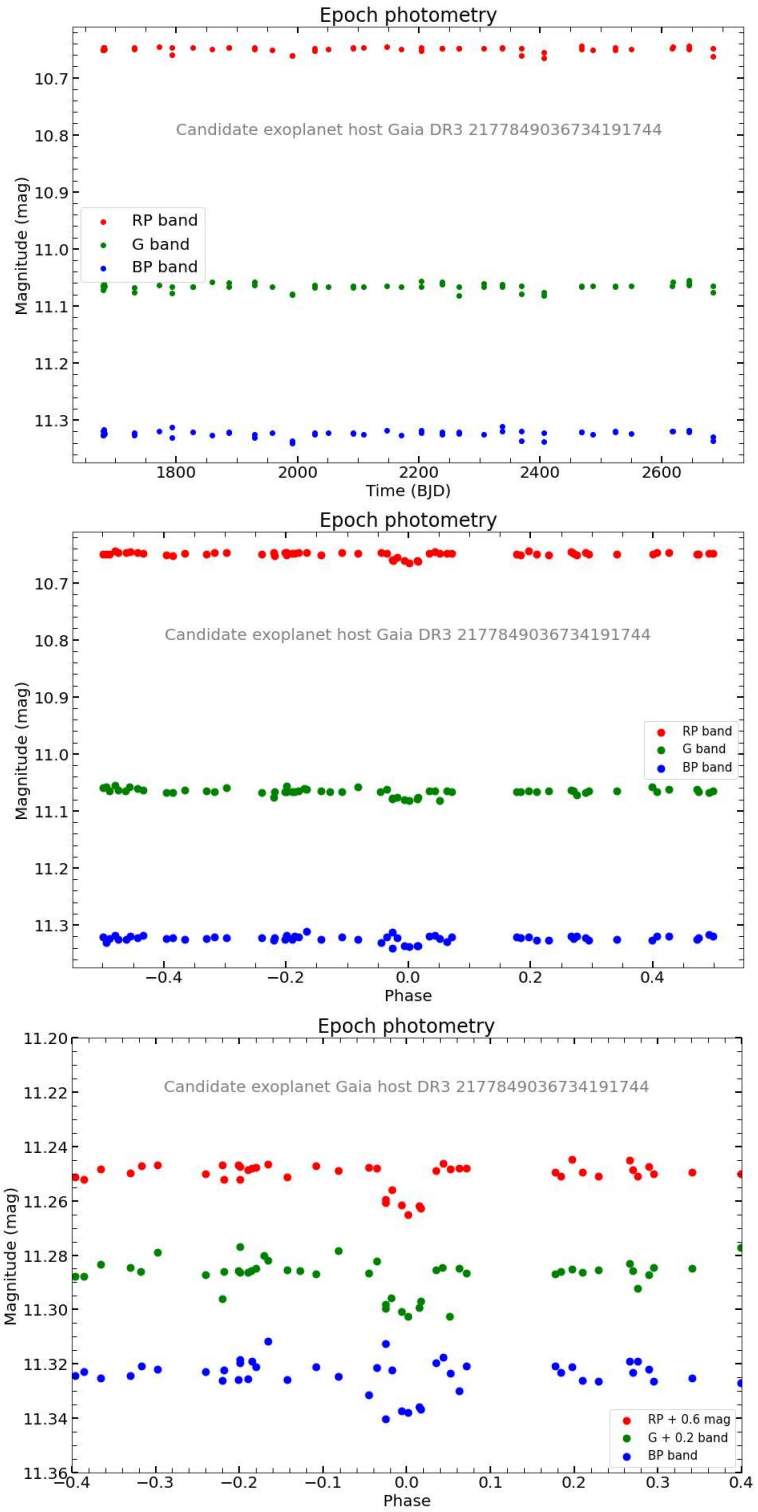

Figure 3.7: Same as figure 3.24 but for the candidate exoplanetary host Gaia DR3 2177849036734191744 (TYC 3970-844-1). The light curves in the middle and bottom panels have been folded according to the period P = 3.81 d.

3.3 Eclipsing binaries

While the majority of stars is in binary systems, only a fraction of them appears to the observer as eclipsing; this family is of capital importance, since eclipsing binaries allow to derive the stars' physical and orbital parameters, play a fundamental role in stellar evolution and their eccentricity can be used as a test for the theory of general relativity. Moreover from variations in the eclipse timings (ETV) the presence of extra-solar planets (circumbinary planets) and/or additional companions in a multiple system can be inferred.
Unresolved eclipsing binaries are a major source of false positive planetary transits and therefore constitute a challenge for transiting planet surveys, although for PLATO brighter targets this issue is minimized.
Gaia DR3 Catalogue contains 813 687 unique non-single star sources between astrometric, spectroscopic, photometric binaries and higher order stellar systems (Arenou et al. 2022 [17]); moreover it includes the largest collection to date (2 184 477 sources) of eclipsing binaries (86 918 of which provided with orbital solutions), whose brightnesses span from a few magnitudes to 20 mag in the Gaia G-band (Mowlavi et al. 2022[18]).
The PLATO Input Catalogue features Algol (β Persei) type (EA), β Lyrae type (EB), and W Ursae Majoris type (EW) eclipsing binaries, distributed between the northern (2 977 sources) and southern (3 466 sources) outer observation fields.

Their distributions in the Aitoff Galactic projection and in the observational Hertzsprung–Russell diagram are shown in figures 3.8 and 3.9 respectively.

It is possible to identify different groups of eclipsing binaries among the sample, from wide (P $>$ 50 d) to tight (P $<$ 10 d) systems, in the orbital period histogram displayed in figure 3.10.

The G, G_{RP} and G_{BP} light curves of the eclipsing binary Gaia DR3 393454948901343360 are shown in figure 3.12, where the gaussian shape of the primary eclipse is clearly visible. A sharp dip in the brightness occurs every 1.72 days when the fainter component star eclipses the brighter one, while a shallower dip occurs when the brighter star eclipses the fainter one.

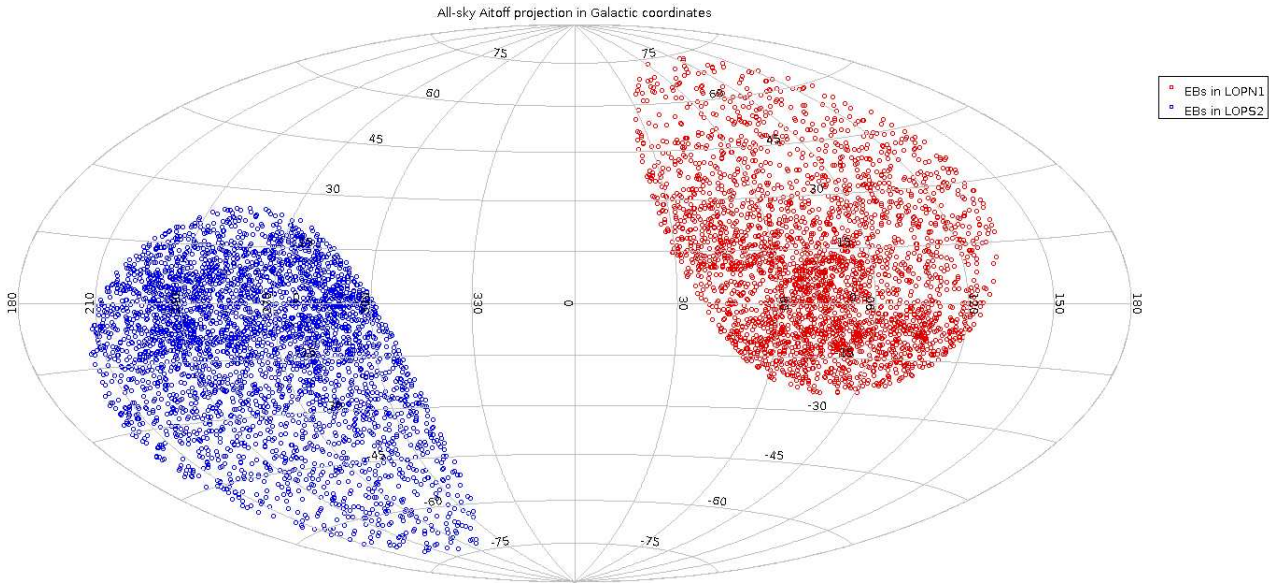

Figure 3.8: Sky map of eclipsing binaries in Galactic coordinates

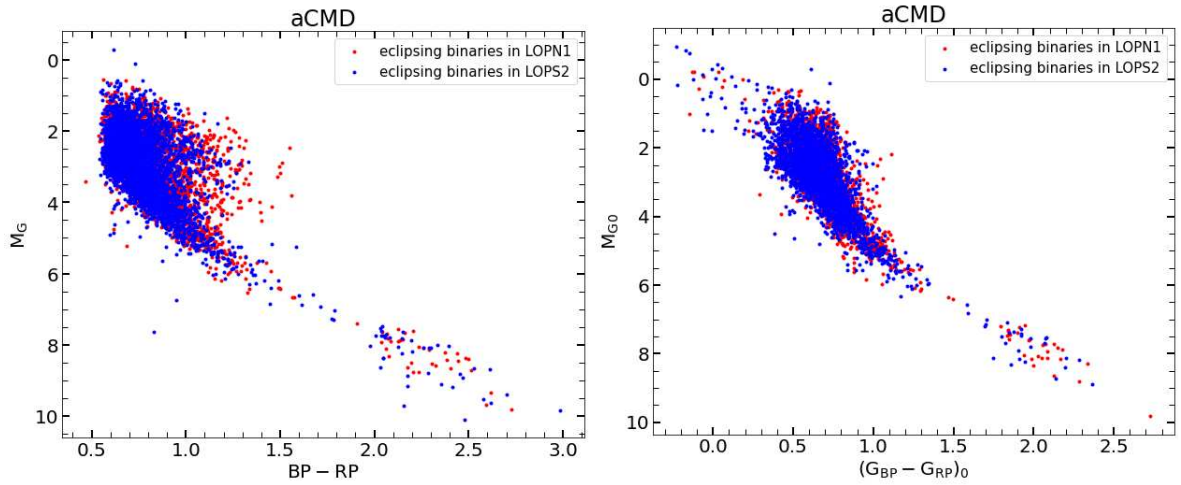

Figure 3.9: Absolute Color-Magnitude diagram (left) and extinction-corrected absolute CMD (right) for the total sample of eclipsing binaries in PIC.

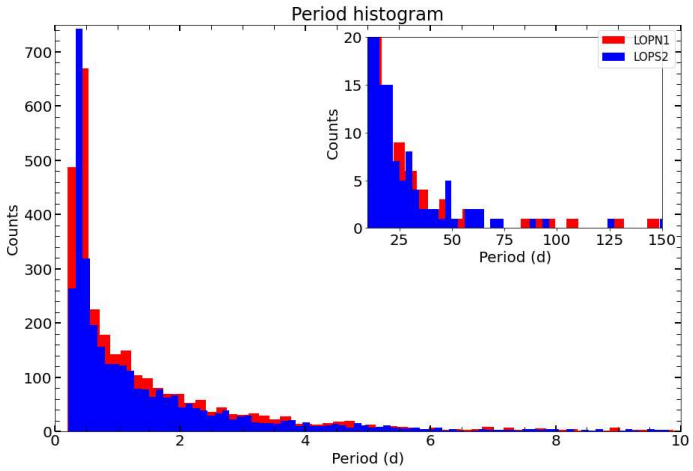

Figure 3.10: Distribution of the orbital periods of the PIC eclipsing binaries.

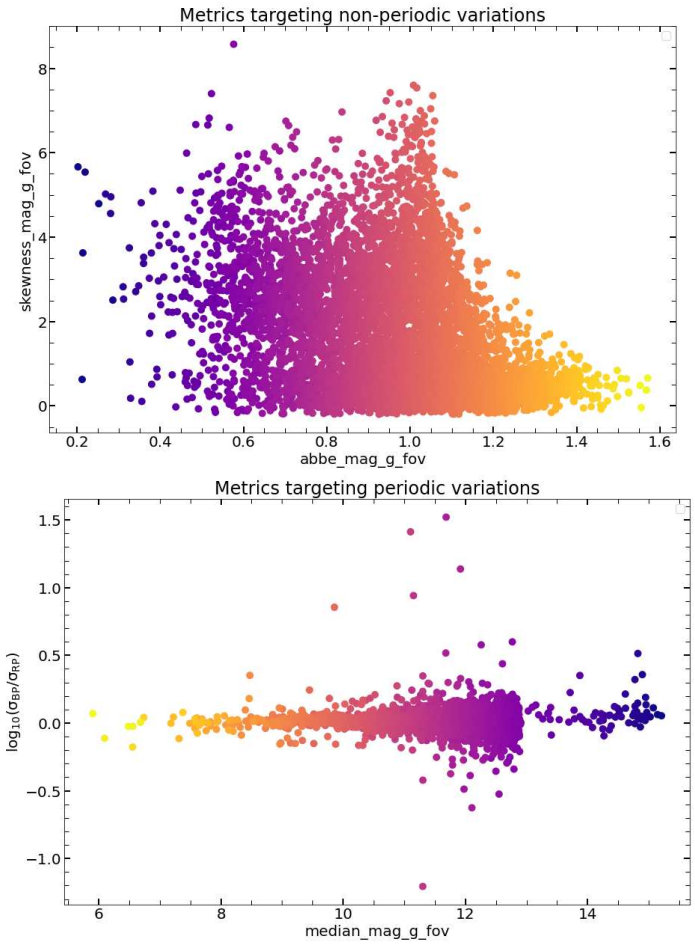

Figure 3.11: Metrics targeting non-periodic (top) and periodic (bottom) variations for the eclipsing binaries.

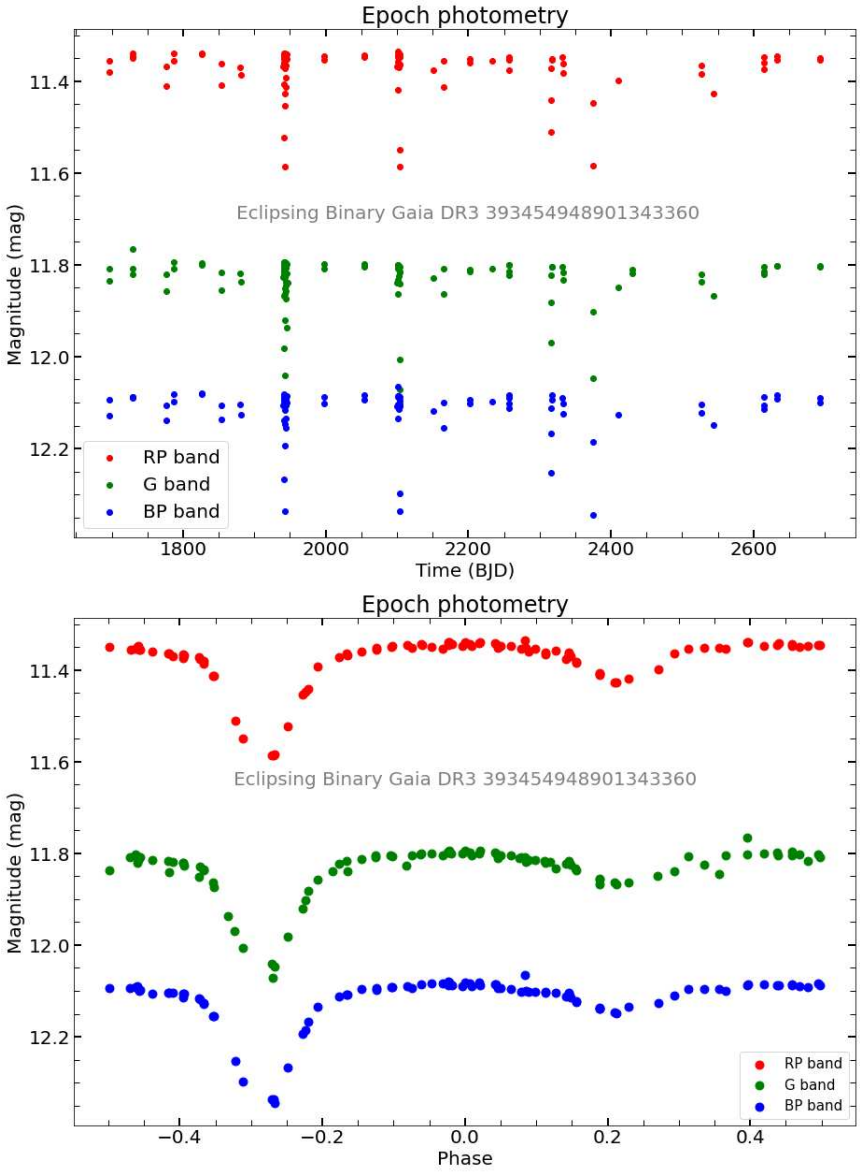

Figure 3.12: Light curve of the eclipsing binary Gaia DR3 3934549489013433 60, in the time domain (top) and folded according to the orbital period P = 1.72 d (bottom).

3.4 Solar-like variables

For this class of solar-like variable stars, the flux variability is induced by the presence and the evolution of magnetically active regions (MARs), such as dark spots and bright faculae (Distefano et al. 2022 [19]). These magnetically active stars present a selection of variability phenomena whose time-scales can range between few minutes, as in the case of flare events and rotation cycle, to years, as in the case of the periodic 11-yrs cycle observed in the Sun. At an intermediate time-scale, solar-like stars' light curves display a rotational modulation signal, which is a quasi-periodic flux variation induced by the stellar rotation that modulates the visibility of MARs over the stellar disk.

The galactic distribution of these variable sources as they are collected in the PLATO Input Catalogue is shown in fig. 3.13: as explained in [11] and [19] the evident peculiar features on the distribution reflect the dependence of the solar-like sources identifications on the number of observations permitted by Gaia's revolving scanning law, and it is therefore an instrumental effect rather than an astrophysical one. We refer to Appendix A.4.2 in [8] for the Galactic Aitoff projection of the simulated number of FoV transits for 5 yr of Gaia scanning law and to Fig. 3 in [11] for the sky map of the least-sampled sources in Galactic coordinates.
In fig. 3.14 we display the reddened and intrinsic absolute CMD.

The photometric amplitude A of the rotational modulation signal can be regarded as a proxy of the stellar magnetic activity level, which increases towards shorter rotation periods together with the MARs lifetime; moreover from the period of the rotational modulation signal the stellar rotation period can be inferred. The relationship between A and P can be observed in the density map reported in fig. 3.15, which shows as expected from the literature [19] the presence of three families of rotating stars, classified as Low-Amplitude-Slow-Rotators (LASR), Low-Amplitude-Fast-Rotators (LAFR), and High-Amplitude-Rotators (HAR).
The rotational modulation signal looses coherence and stability across the full Gaia photometric time-series because of the intrinsic evolution of MARs and can be detected only in shorter sub-series, whose duration is comparable with the spots life-time. Therefore when

analyzing epoch photometry it is necessary to perform a segmentation of the time-series, where each segment presents a significant period according to which the light curve can be folded. This can be observed in fig. 3.17, where the light curve of the solar-like star Gaia DR3 5737431512607241600 is displayed.

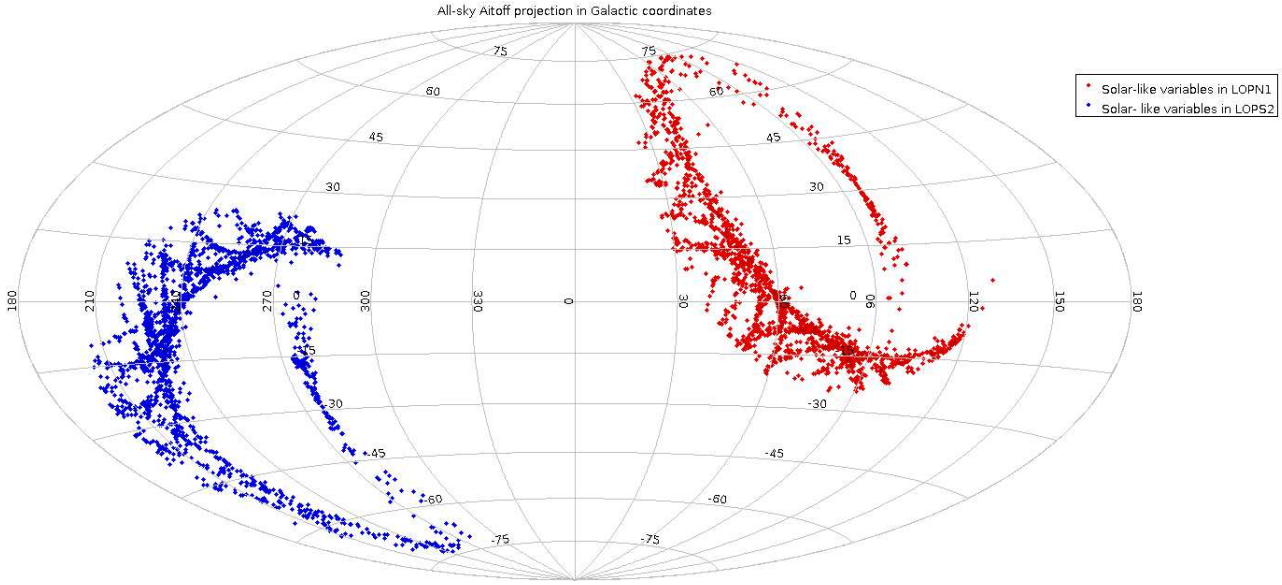

Figure 3.13: Sky map of solar-like variable stars in Galactic coordinates.

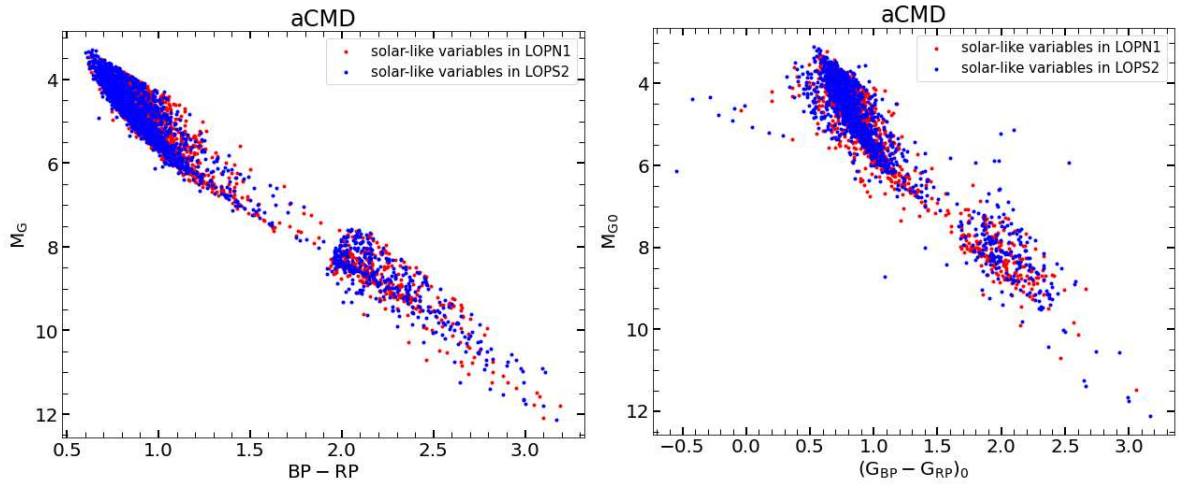

Figure 3.14: Absolute Color-Magnitude diagram (left) and extinction-corrected absolute CMD (right) of the total sample of solar-like variables in PIC.

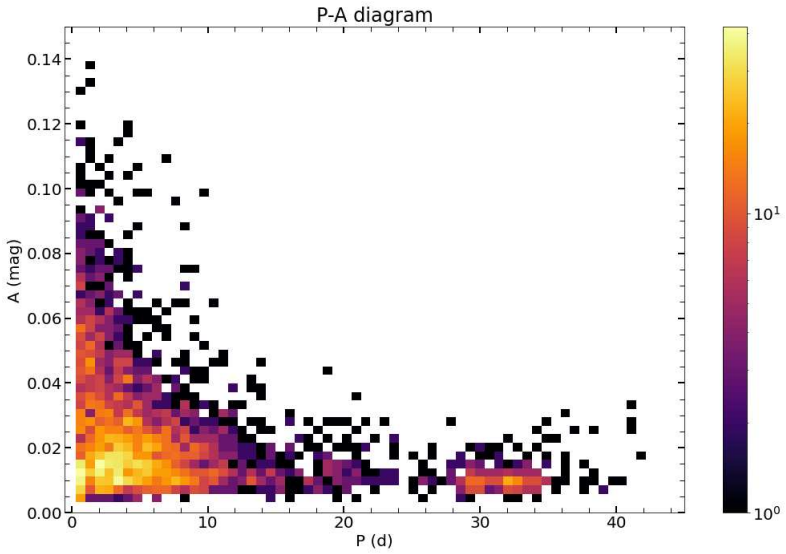

Figure 3.15: Period-Amplitude diagram for the total sample of solar-like variables in PIC.

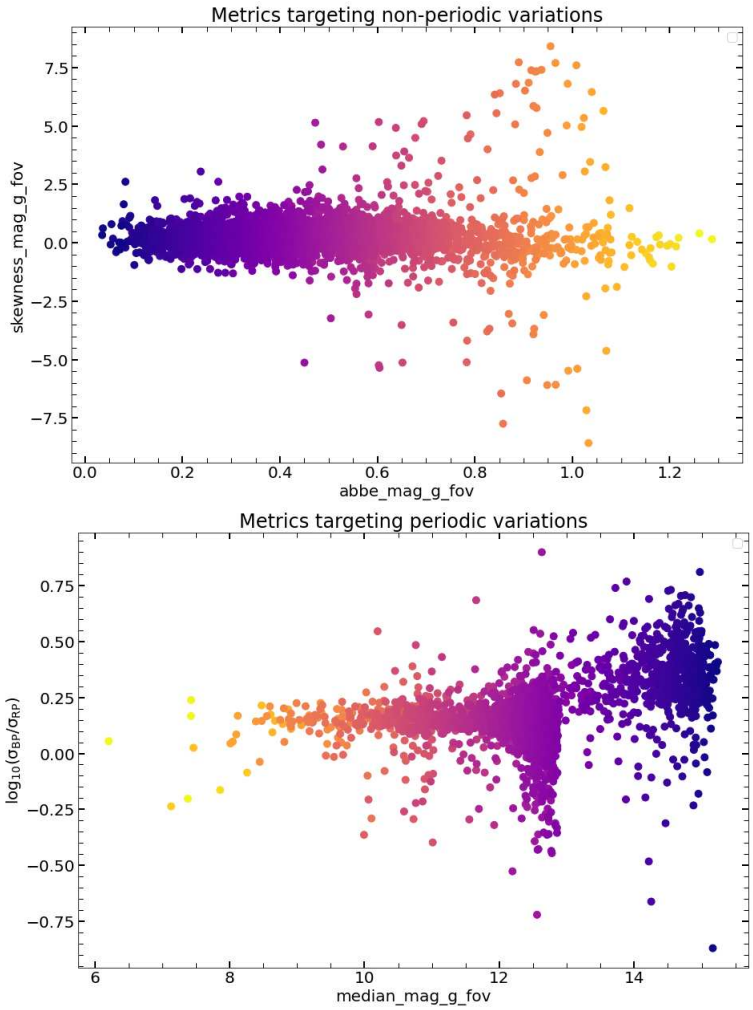

Figure 3.16: Metrics targeting non-periodic (top) and periodic (bottom) variations for solar-like rotators.

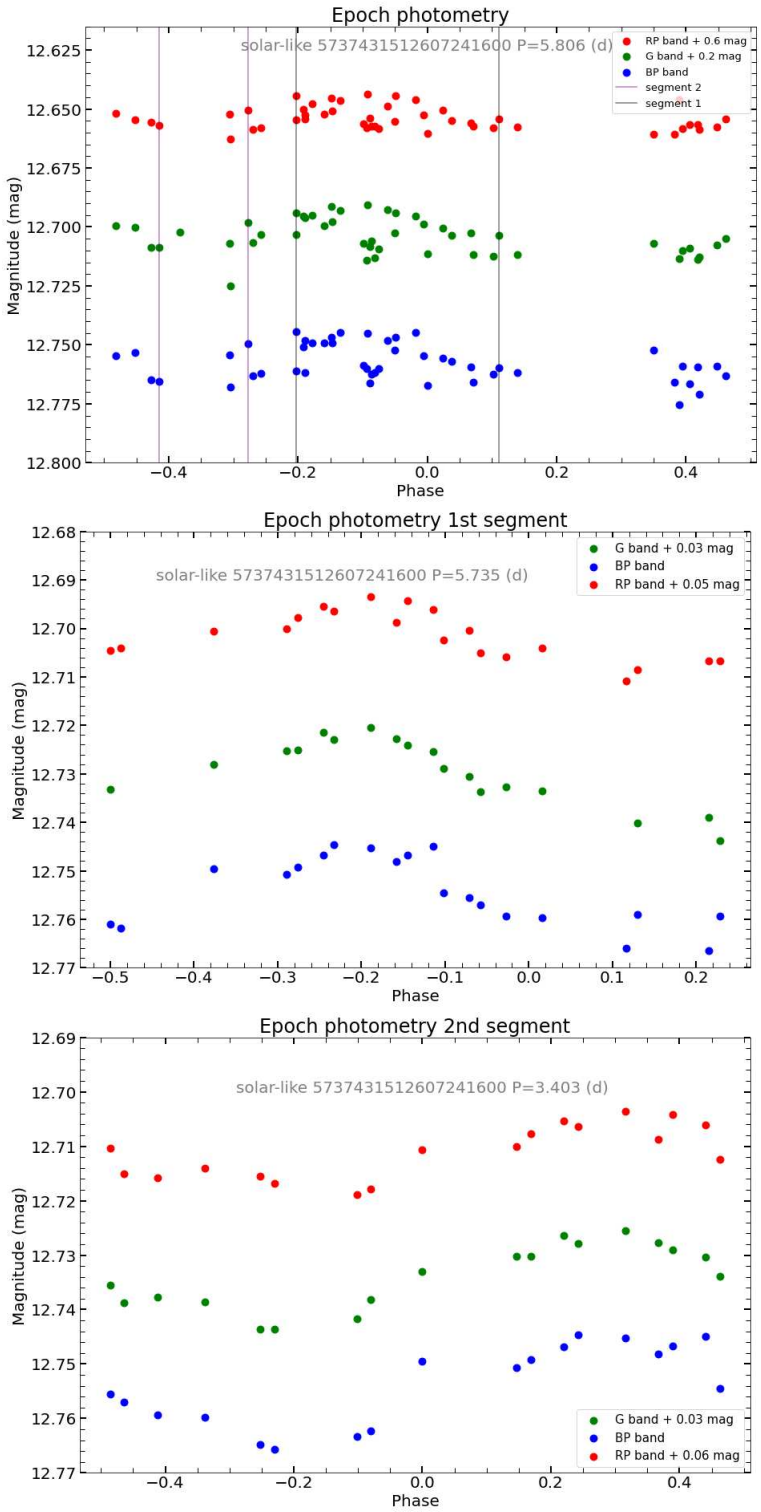

Figure 3.17: Top panel: full G, G_{BP} and G_{RP} time-series for the solar-like source Gaia DR3 5737431512607241600 folded over the best rotation period P = 5.806 d, where the vertical lines enclose the segmentation. Middle panel: first sub-series folded according to the segment period P = 5.735 d. Bottom panel: second sub-series folded over the segment period P = 3.403 d.

3.5 Main Sequence oscillators

This sample of variable sources collected in the PLATO Input Catalogue include intermediate-to-high mass upper Main Sequence pulsators ($M \geq 1.3 M\odot$); among them SX Phoenicis, γ Doradus and δ Scuti stars can be distinguished, the latter being the most populated variability class.

These non-radial oscillators are often multi-periodic, display very low amplitudes and typically a significant frequency peak can be observed in the Fourier spectrum of their Gaia light curve, associated to a dominant oscillation mode (De Ridder et al. 2023 [20]). They present stable oscillations with "pressure modes" excited in a stochastic way by turbulent convection in the external envelope; a particularly promising tool to investigate their internal physics and estimate their ages is asteroseismology, which will derive observational constraints on the rotation of the stellar core, where "gravity modes" are confined.

The sky map distribution of the considered sample of upper-MS oscillators is reported in figure 3.18, where an over density can be noticed on the Galactic plane, as it is to be expected for young objects; the sources distribution in Hertzsprung-Russell (HR) diagram is shown in figure 3.19.

In fig. 3.20 and 3.21 the distribution of the photometric amplitude in the G-band as a function of the primary frequency, and the histogram of the primary frequency can be observed respectively.

From the literature [20] δ Scuti stars are known to exhibit an empirical relation between their period and their luminosity: the period- Wesenheit G index diagram for our sample of stars is reported in figure 3.22, which shows two main clusters of pulsators presenting different oscillation regimes. The difference between fast rotating pulsators and slow-to-moderate pulsators arises from the physics of their internal rotation and core convection.

Moreover, from the photometric G-band amplitude - projected rotational velocity plot displayed in fig. 3.23 it can be observed that stellar rotation attenuates the amplitude of the dominant oscillation mode of δ Sct stars, as expected: indeed even from the reduced available sample of stars provided with rotational velocity measurements, it appears that high ampli-

tude sources tend to rotate slower, while the oscillation amplitude decreases for increasing rotational velocities.

The full time-series in the G, G_{BP} and G_{RP} bands for the star Gaia DR3 39332606552108761 and the phase diagram for the same source folded according to its primary frequency are displayed in figure 3.25.

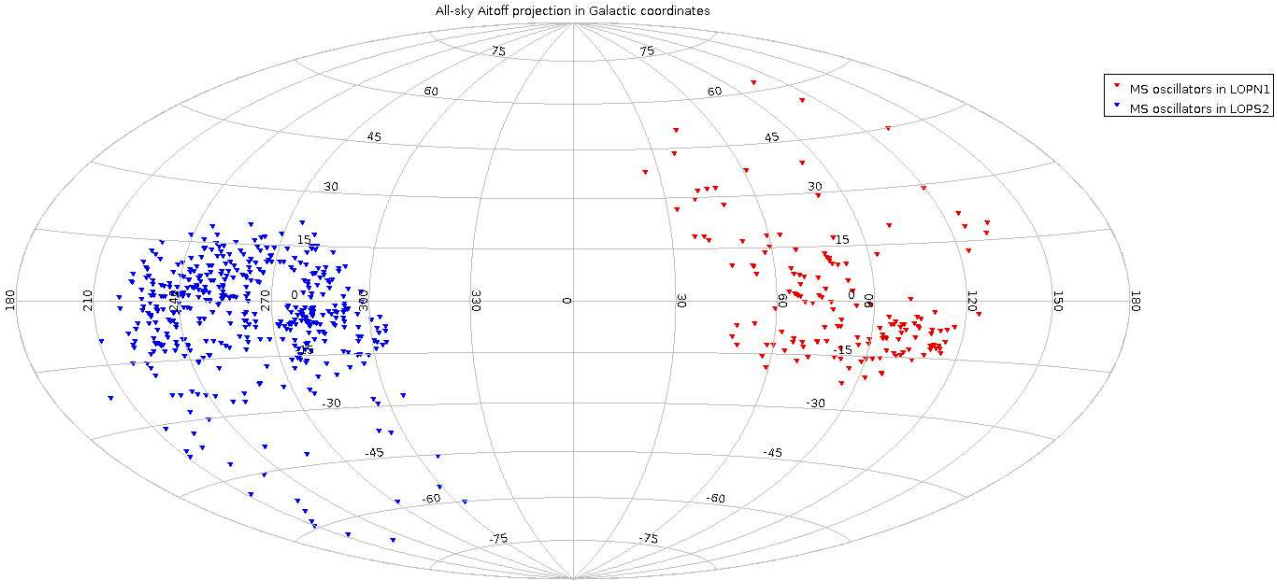

Figure 3.18: Sky map of Main Sequence oscillators in Galactic coordinates

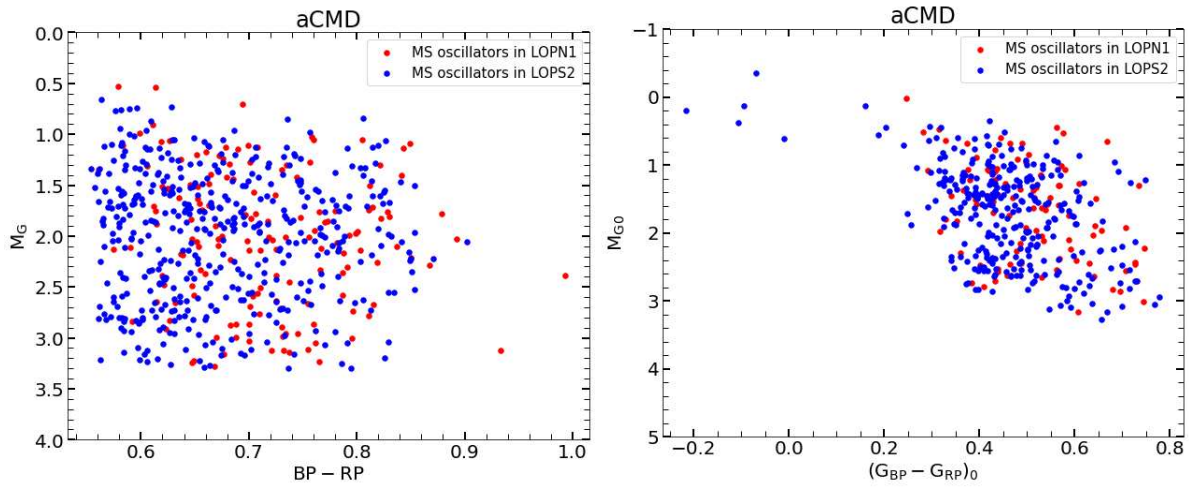

Figure 3.19: Absolute Color-Magnitude diagram (left) and extinction-corrected absolute CMD (right) for the total sample of MS oscillators in PIC.

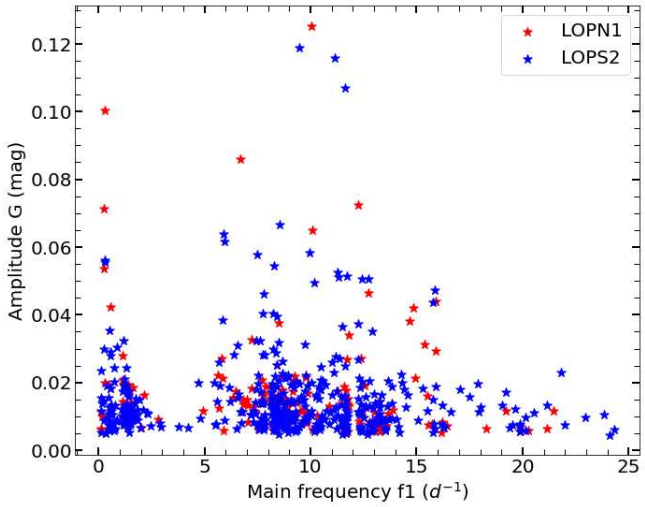

Figure 3.20: G-band amplitude-main frequency distribution

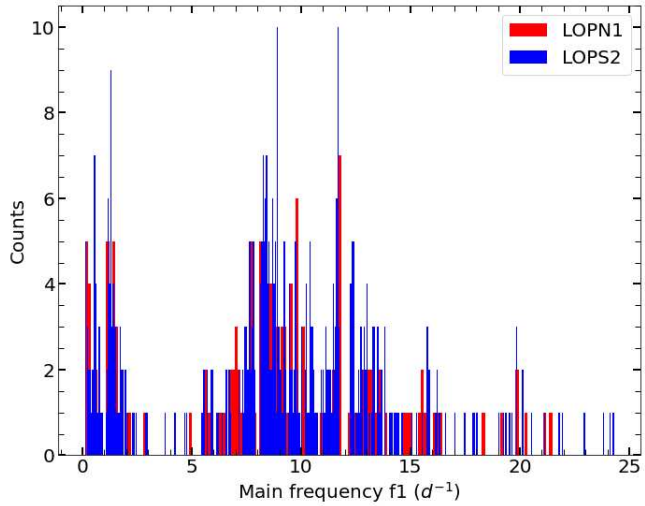

Figure 3.21: Histogram of the primary frequency for the upper-MS pulsators of both LOP fields.

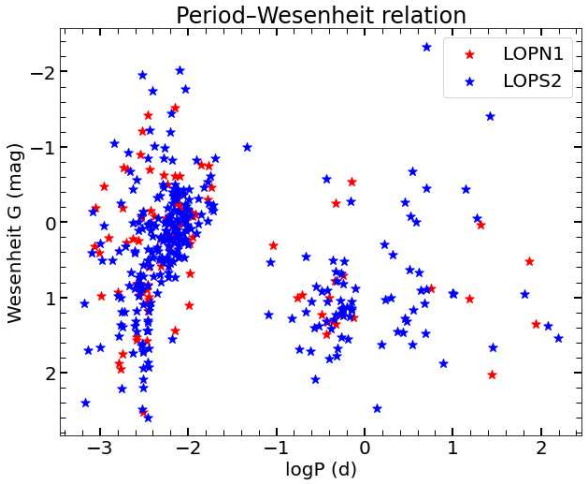

Figure 3.22: Period-Wesenheit G diagram for the upper-MS pulsators of both LOP fields.

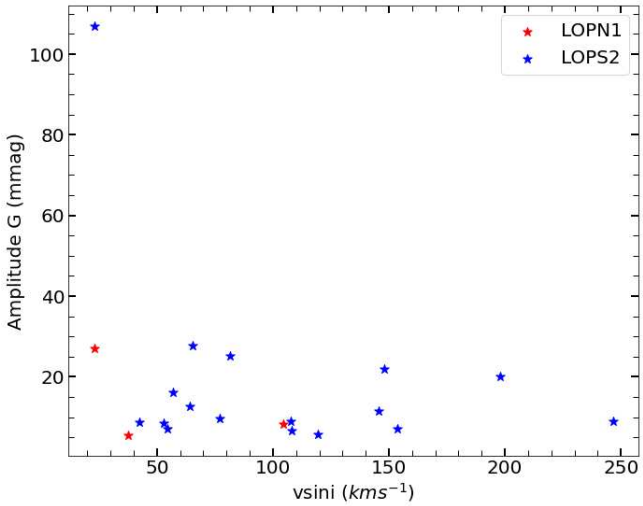

Figure 3.23: Photometric amplitude A in the Gaia G-band as a function of the projected rotational velocity for a sample of δ Sct stars.

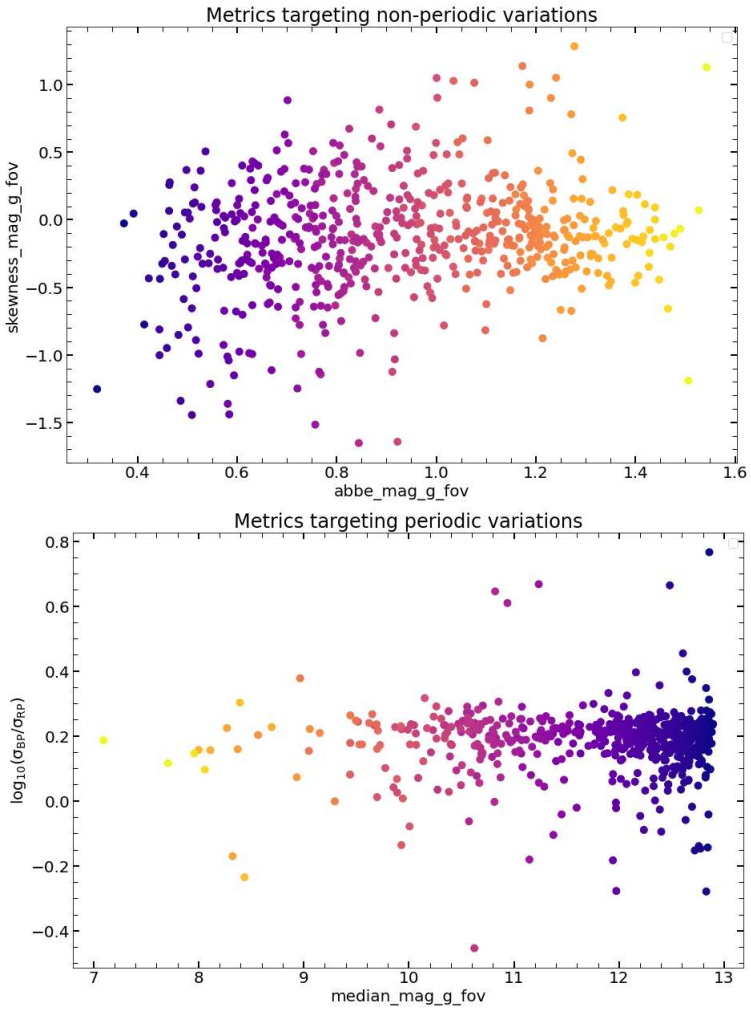

Figure 3.24: Metrics targeting non-periodic (top) and periodic (bottom) variations for the MS oscillators.

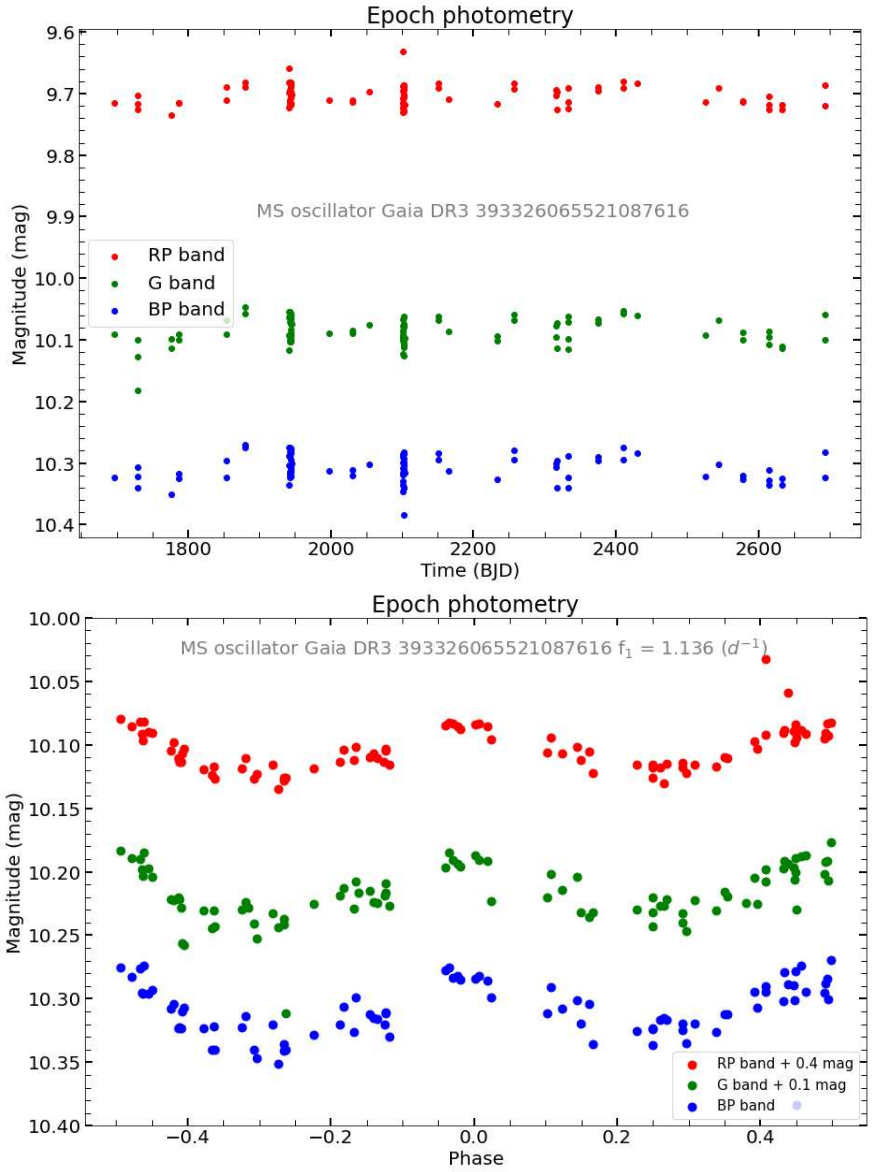

Figure 3.25: Top: photometric time series for the pre MS oscillator Gaia DR3 393326065521087616 in the G, G_{BP} and G_{RP} bands. Bottom: phase diagram for the same source folded according to its primary frequency.

3.6 RR Lyrae

RR Lyrae stars are a class of pulsating Horizontal Branch stars known to be excellent distance indicators due to the strong correlation between their absolute magnitude and metallicity, and therefore are used as standard candles for measuring (extra-)galactic distances. They are also regarded as tracers of the chemical and dynamical properties of the oldest observable population of stars, and are typically low mass ($M \approx 0.6\text{-}0.8\ M_{\odot}$), old (ages $>$ 9-10 Gyr) and metal-poor stars whose surface expands and contracts regularly with periods shorter than a day (Clementini et al. 2022 [21]).

RR Lyrae stars can be subclassified into RRab, RRc and RRd depending on their pulsation mode, respectively called fundamental, radial first overtone and double mode (the latter is given by the superposition of the other two ones excited simultaneously).

The ab-type RR Lyrae stars oscillate with periods typically between about 0.42 d and 1 d, their light curves look asymmetrical and sawtooth-shaped (sharp rising portions and slow declines) and present a variation in brightness of up to one magnitude in the *Gaia* visual G band, while c-type RR Lyrae stars have periods between about 0.2 d and 0.42 d, symmetric and almost sinusoidal light curves and brightness variations of up to about half a magnitude in the visual band.

The PLATO Input Catalogue features 3 RRc stars and 81 RRab stars in the northern outer LOP field, and one RRd star, 8 RRc stars and 69 RRab stars in the southern outer LOP field. In fig. 3.26 the sky map distribution of these periodic pulsating sources can be observed, while fig. 3.27 displays the absolute colour-magnitude diagram corrected for extinction for the RR Lyrae stars of both galactic hemispheres. From the plot it results that four sources are shifted with respect to the Horizontal Branch; this is very likely due to a mismatch in the Gaia processing pipeline, which may have erroneously assigned them to the wrong variability class. Indeed, from [11] we are aware that solar-like candidates such as BY Draconis variables may be found among the false positives of the RR Lyrae Gaia DR3 SOS module; this is the case of the source V* V552 Car (GDR3 5239771349915805952), which the SIMBAD database [10] reports

[10] See `http://simbad.u-strasbg.fr/simbad`.

as "misclassified RR Lyrae in Gaia DR3". Additionally, Gaia provides for each astrometric source a quality indicator called Renormalized Unit Weight Error (RUWE), which is also a robust metric for unresolved multiplicity; typically a threshold of RUWE < 1.4 indicates well-behaved single-star astrometric solutions. As it is shown in table 3.6, among the four misplaced sources in the color-magnitude diagram, two present very high values of RUWE and one is borderline; we are therefore quite confident of the poor accuracy of the astrometric solution for at least two of these stars, which may have caused a mistake in the classification of their variability.

source_id	parallax	parallax_error	RUWE
1583952778778092928	2.40	0.01	1.09
3062985235999231104	3.67	0.02	1.35
5239771349915805952	6.95	0.10	8.66
5352984420098880768	9.14	0.11	10.14

Table 3.6: Astrometric solution for the candidate RR Lyrae stars.

Fig. 3.28 shows the P-A diagram of the pulsation period and the peak to peak amplitude of the light variation in the G band for the total considered sample of RR Lyrae stars, where the sources have been colour-coded according to their metallicity; it appears that the sources with a longer period present lower values of metal abundance. From figure 3.29 (top) it appears that the mean of the magnitude skewness distribution is negative, as it is to be expected for a sample mostly composed of ab-type RR Lyrae stars, whose lightcurves are asymmetrical (they spend more than 50% of their variability cycle fainter than their mean magnitude). The periodic pulsating nature of RR Lyrae can be inferred also from 3.29 (bottom), that shows the ratio of the two bands variances to be almost constant as a function of the median magnitude per FoV in the G band, with an abrupt increase towards fainter magnitudes probably caused by a noise saturation.

The lightcurves of two arbitrary RR Lyrae stars from our sample are collected in figure 3.30, where the typical saw-tooth shape of the RRab class and sinusoidal shape of the RRc class can be respectively observed. The radial velocity time series of the sources RRab Gaia DR3 2926381228470699392 and RRc Gaia DR3 1956531880222667904 are displayed in figure 3.31;

the RV curves have been obtained by folding the data with the periods inferred from the G-band photometry and it can be noticed that they have the typical shape compared to the light curves, with the minimum value in RV corresponding to maximum star brightness.

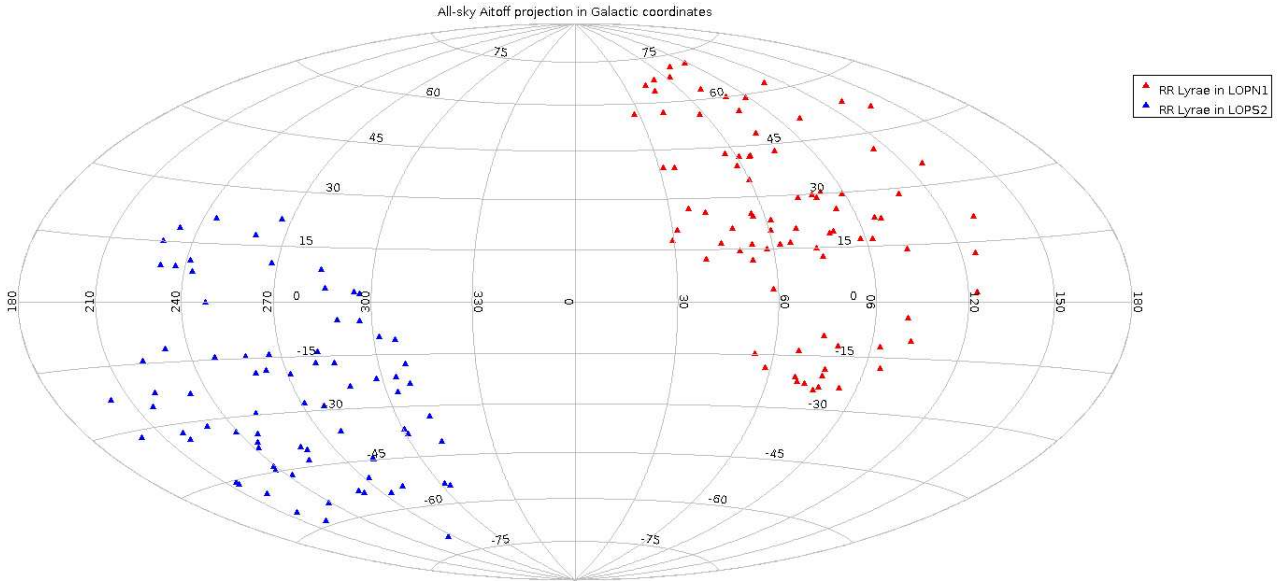

Figure 3.26: Sky map of RR Lyrae stars in Galactic coordinates

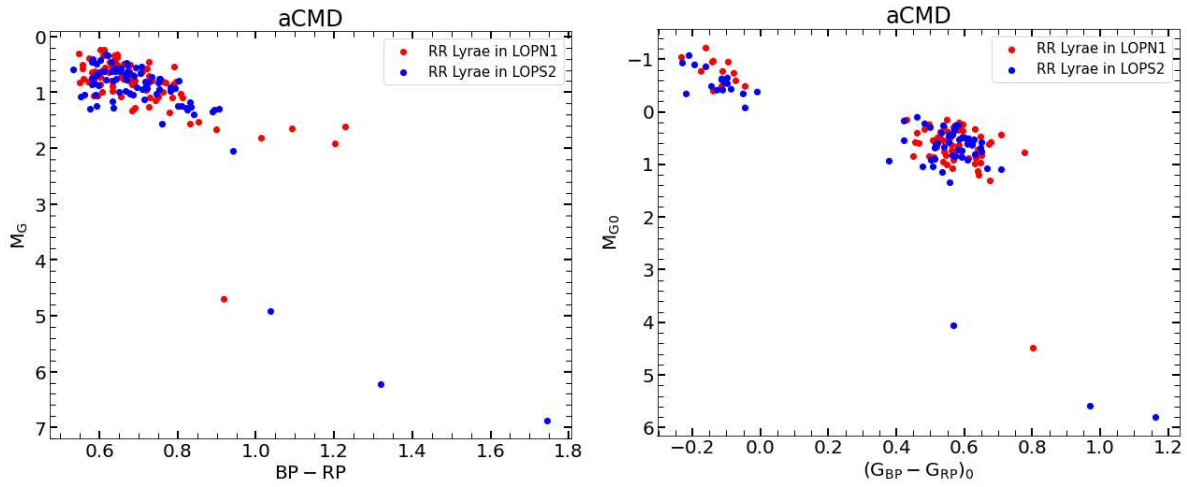

Figure 3.27: Absolute Color-Magnitude diagram (left) and extinction-corrected absolute CMD (right) for the total RR Lyrae sample in PIC.

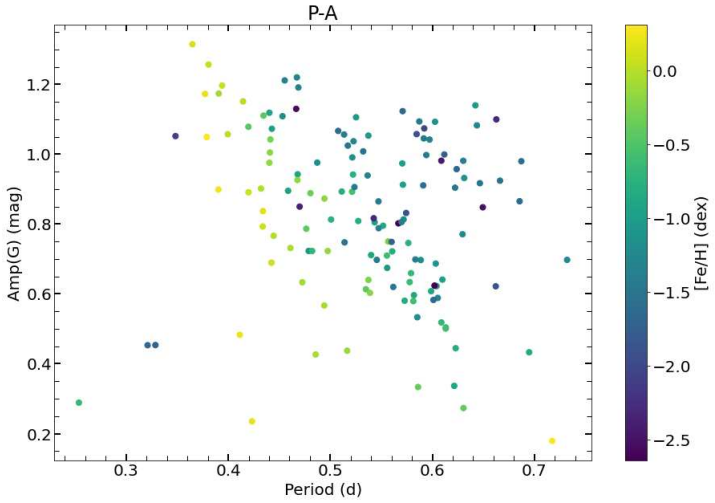

Figure 3.28: Period - Amplitude diagram for RR Lyrae stars colour-coded according to their metallicity

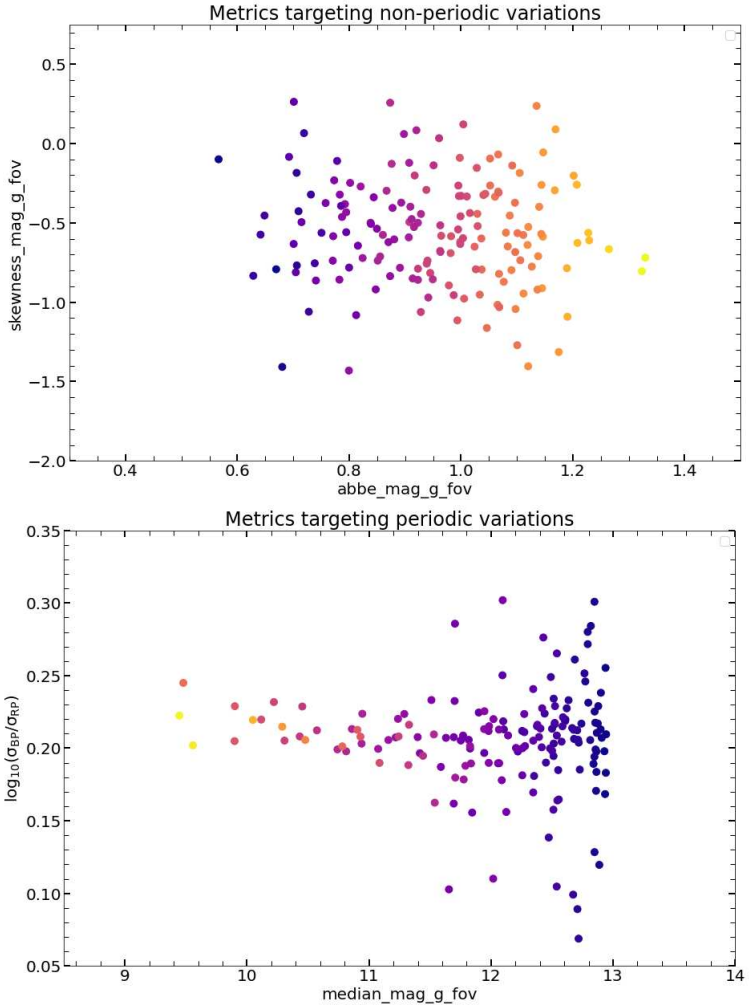

Figure 3.29: Metrics targeting non-periodic (top) and periodic (bottom) variations for RR Lyrae.

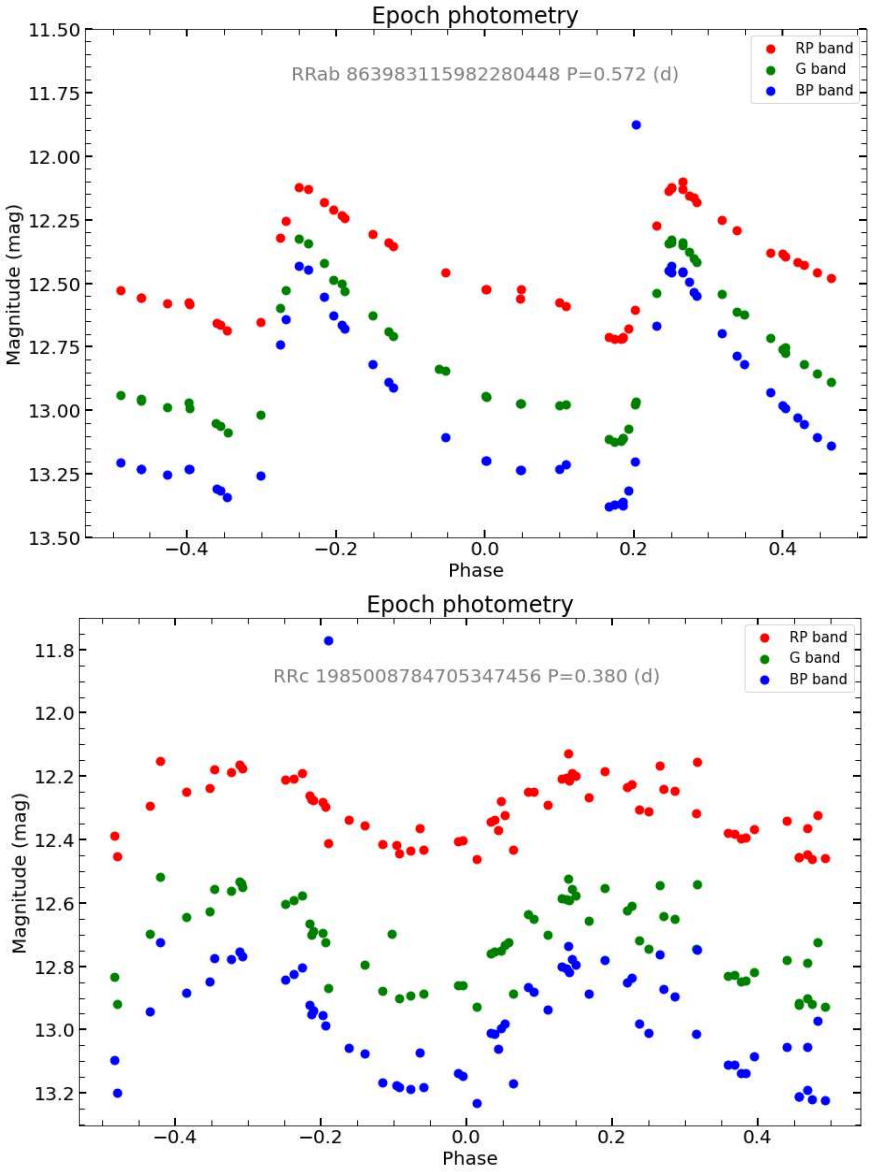

Figure 3.30: Epoch photometry of the ab-type RR Lyrae Gaia DR3 863983115982280448 (top) and of the c-type RR Lyrae Gaia DR3 1985008784705347456 (bottom) in the G, G_{BP} and G_{RP} bands in the phase domain.

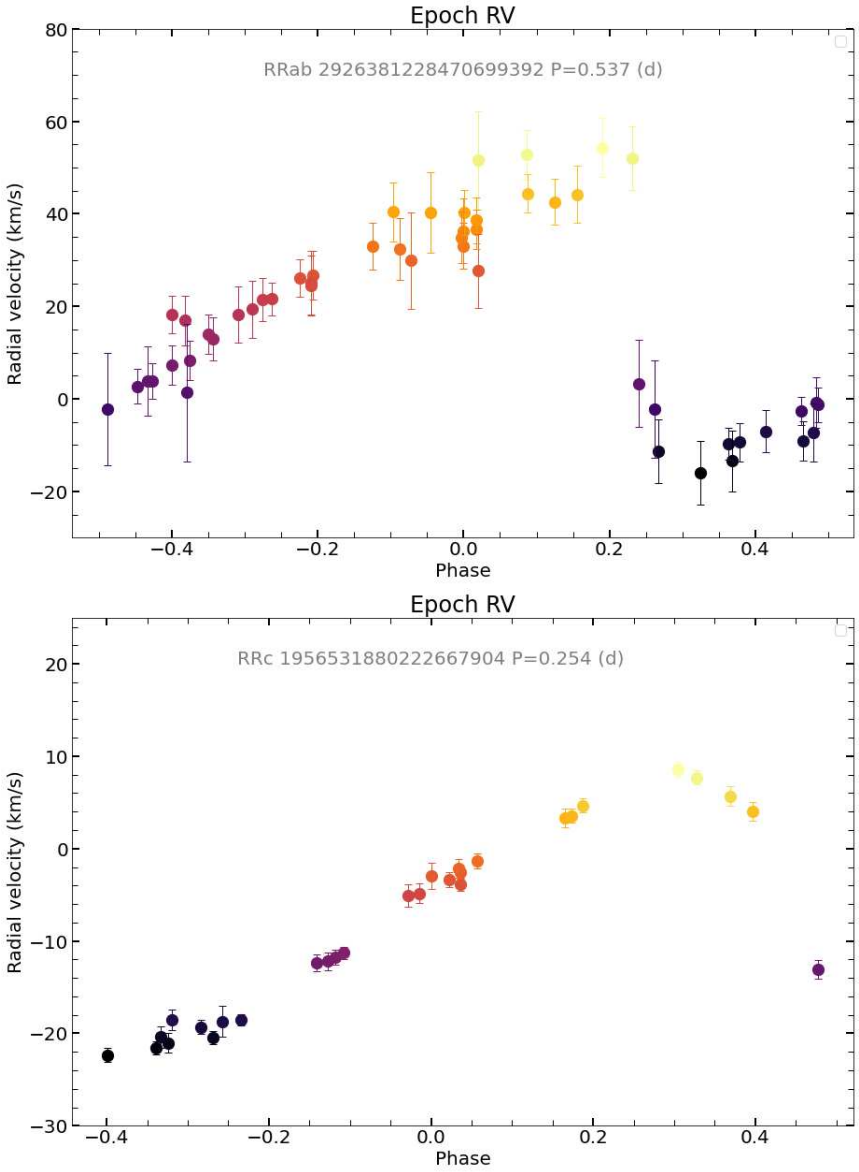

Figure 3.31: Epoch radial velocity of the ab-type RR Lyrae Gaia DR3 2926381228470699392 (top) and of the c-type RR Lyrae Gaia DR3 1956531880222667904 (bottom) in the phase domain.

3.7 Cepheids

Cepheids are a class of periodic variable objects marked by a strong correlation between their absolute magnitude and period[11], which makes them standard candles to measure extra galactic distances, similarly to RR Lyrae stars. They can be classified as classical Cepheids (δ Cep), type II Cepheids (T2CEPs) and anomalous Cepheids (ACEPs).
The first family is the most populated and significant one: δ Cep are typically luminous, young (50-500 Myr) and massive (M $\approx$ 3–11 $M\odot$) stars, that can be used to test stellar evolution models, trace the metallicity gradient of the Milky Way, and model the galactic thin disc (Ripepi et al. 2022 [22]).

Among 15 000 Cepheids included in the Gaia DR3 variable objects collection, only one of them figures in the PLATO Input Catalogue, as it is to be expected since the PIC mainly focuses on less massive FGKM stars: this source is the δ Cep Gaia DR3 4301612233202961024, whose first overtone pulsation period is P = 0.219 d and its mass is $M = 2.418^{+0.040}_{-0.060} M\odot$[12].

Its photometric time series and phase-folded lightcurve are displayed in figure 3.32.

[11] Henrietta Swan Leavitt's observations of variable stars in the Small Magellanic Cloud were the basis for the pulsation period - intrinsic luminosity relation for Cepheids.

[12] This value can be found in the Gaia Archive and has been obtained by the Final Luminosity Age Mass Estimator (FLAME) for Gaia sources.

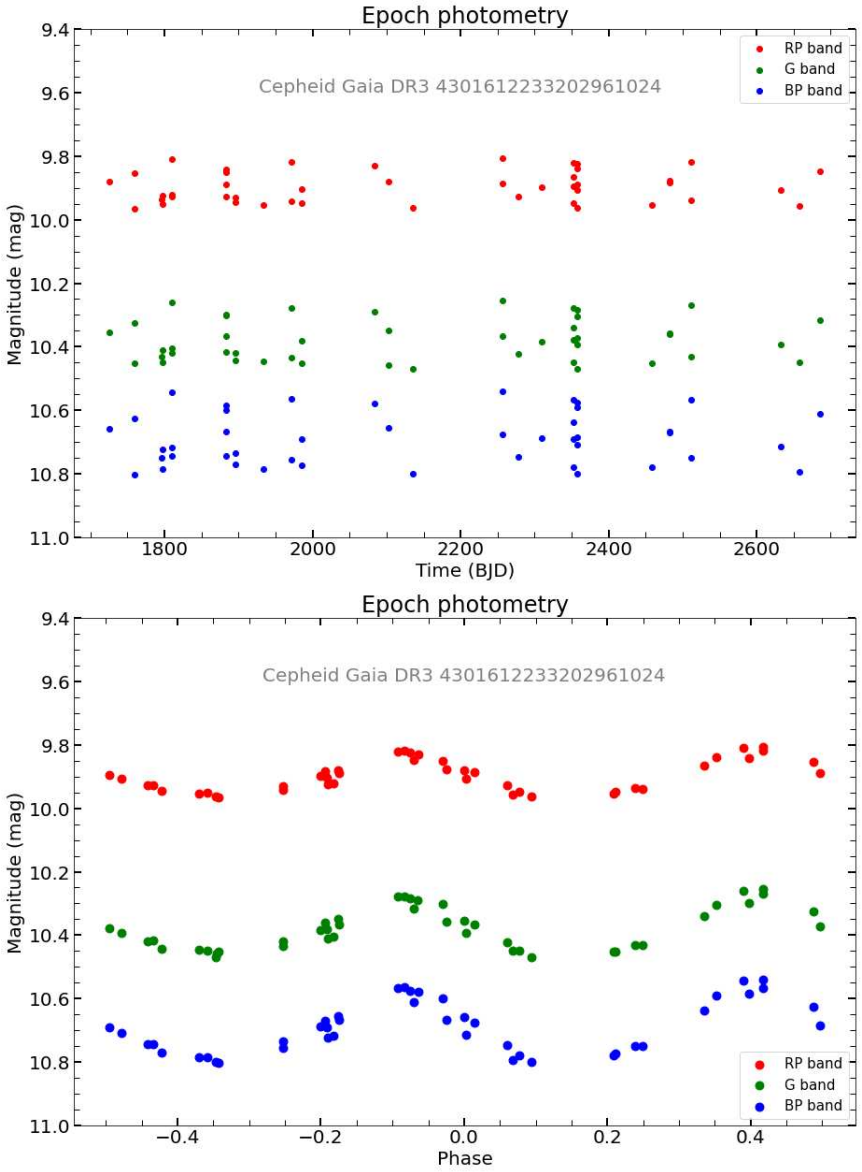

Figure 3.32: Time series (top) and phase-folded lightcurve (bottom) in the G, G_{BP} and G_{RP} bands for the Cepheid Gaia DR3 4301612233202961024 over the first overtone period P = 0.219 d.

3.8 Short timescale variables

The PLATO Input Catalogue counts over seven thousands objects that exhibit very fast variability, with periods ranging from 20 minutes to a day[13] and amplitudes ranking from a few millimagnitudes to a few magnitudes. These short-timescale variable sources are classified as EW-type eclipsing binaries, post-common envelope binaries (PCEB), cataclysmic variables (CV), RRab Lyrae stars, solar-like variables (rotational modulation, BY Draconis, RS Canum Venaticorum stars) and Main Sequence oscillators such as δ Scuti stars.

Gaia provides an exceptional opportunity for comprehensive fast-variability studies over the whole sky, with its sparse sampling in the G band and its high photometric precision; similarly the rapid observing cadence of PLATO makes it ideal for studying these very short period objects. Roelens et al. 2018 [23] identified the candidates to be included in the Gaia DR3 *short_timescale* SOS module via variogram analysis; this method quantifies the magnitude variations between photometric measurements as a function of the time lag between them and defines a detection threshold above which the variability is significant enough at time lags shorter than 12 h.

The all-sky map in Aitoff projection and Galactic coordinates of the PLATO Input Catalogue's short timescale variables is shown in figure 3.33, while fig. 3.34 displays the observational Hertzsprung-Russell diagram corrected for extinction. In figures 3.35 and 3.36 the amplitude-frequency plot and the periods distribution are reported. The regular pattern that can be observed with peaks around multiples of 4 d^{-1} is due to the spin frequency of the spacecraft, as Gaia's nominal scanning law secures a 6 h rotation period [23].
The lightcurves in time and phase domain of the short-timescale eclipsing binary Gaia DR3 4594961454434214144 are reported in figure 3.38.

[13]Sources with periods between 0.5 and 1 d are considered 'extended' short-timescale variables.

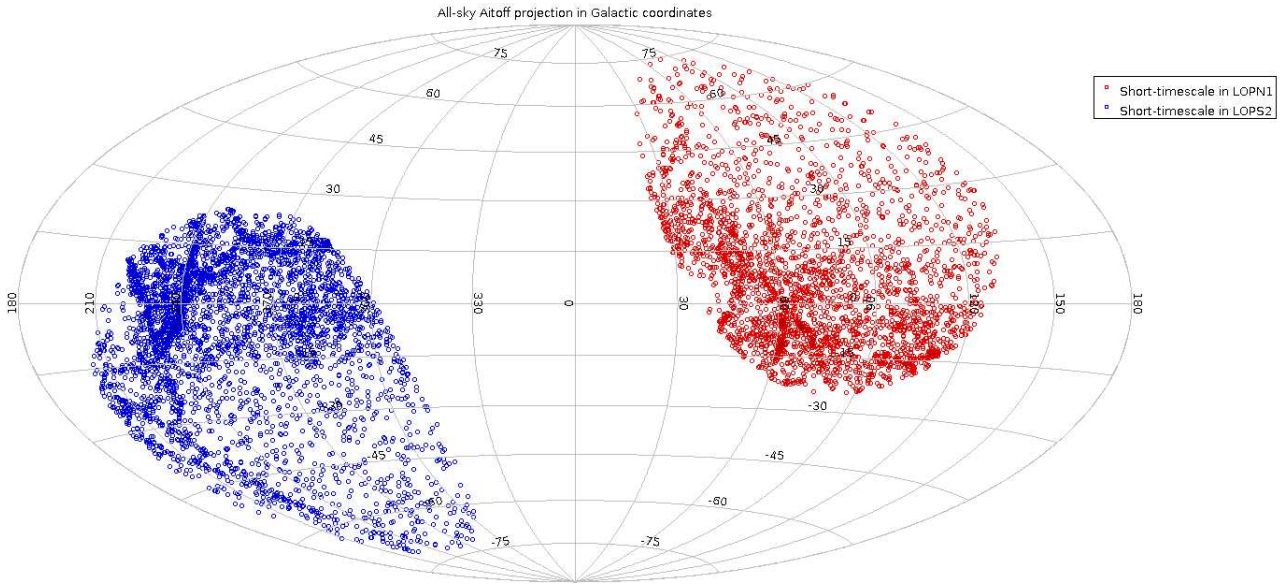

Figure 3.33: Sky map of short-time variables in Galactic coordinates.
The imprint of the Gaia scanning law and the effect of selecting sources with more than 20 FoV transits is clearly visible, as pointed out in [11] and [23].

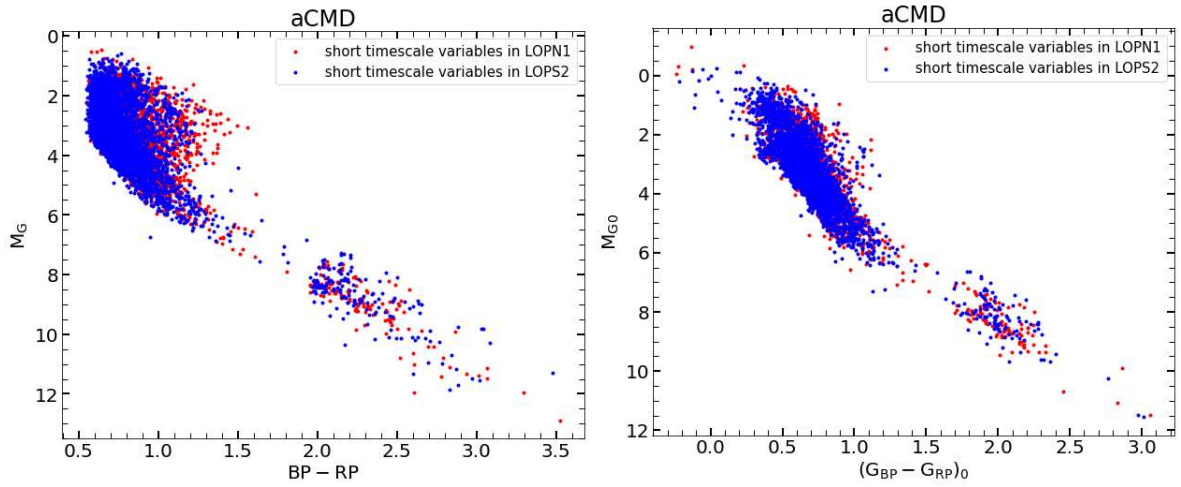

Figure 3.34: Absolute Color-Magnitude diagram (left) and extinction-corrected absolute CMD (right) for the total sample of short timescale variables in PIC.

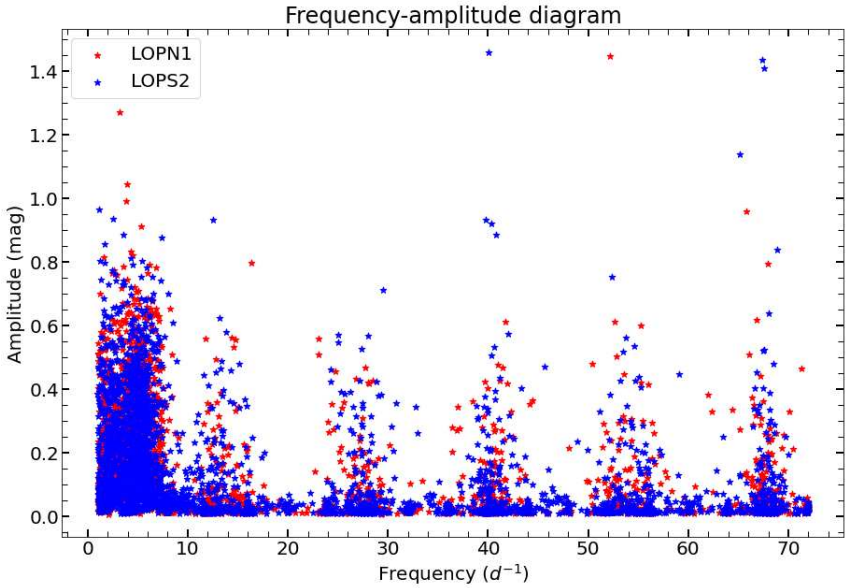

Figure 3.35: Frequency-amplitude distribution for the short-timescale variables in PIC.

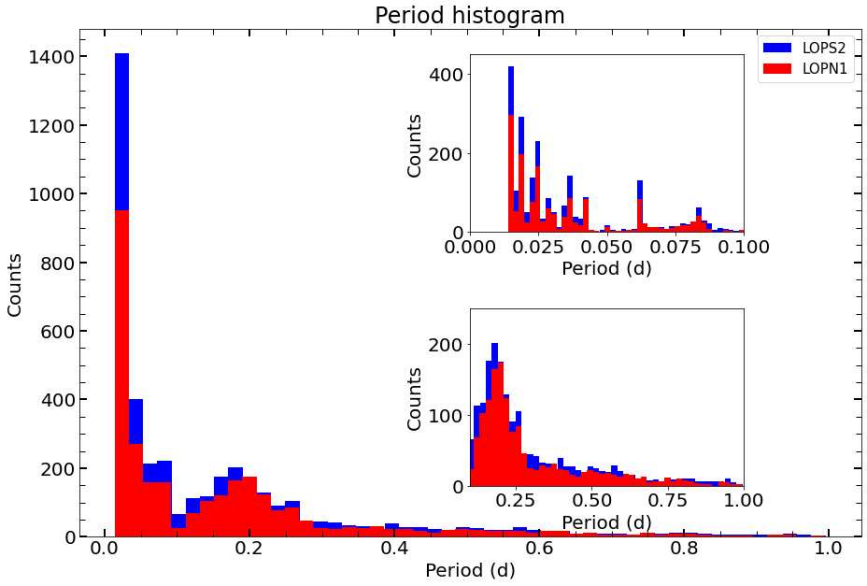

Figure 3.36: Period distribution for the short-timescale variables in PIC.

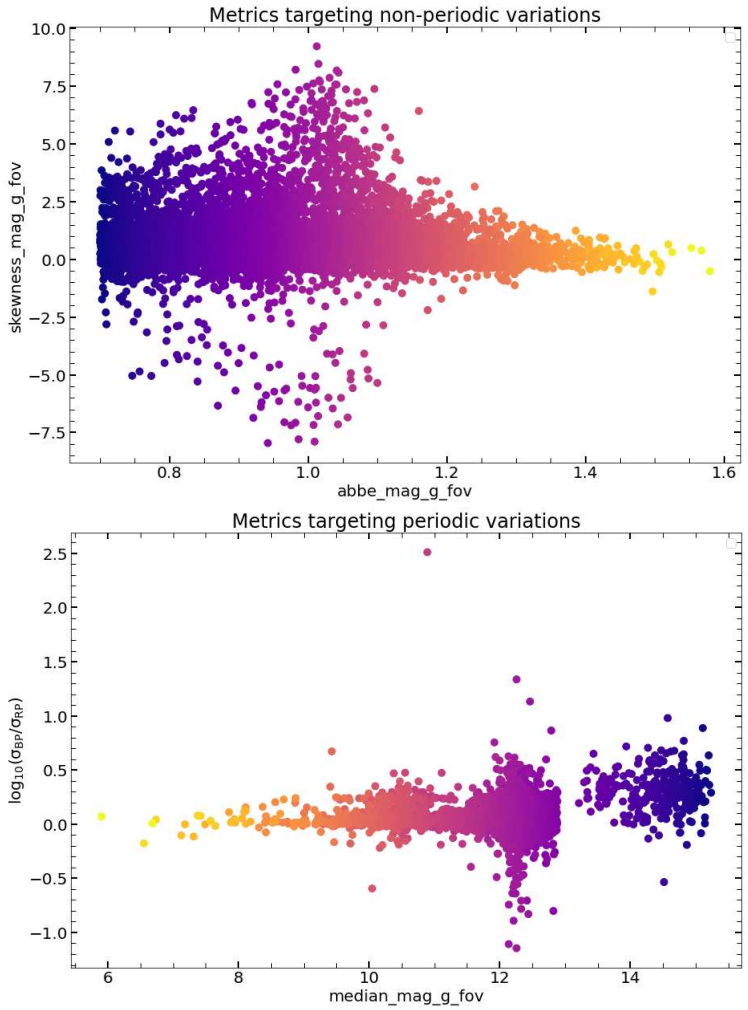

Figure 3.37: Metrics targeting non-periodic (top) and periodic (bottom) variations for short-timescale variables.

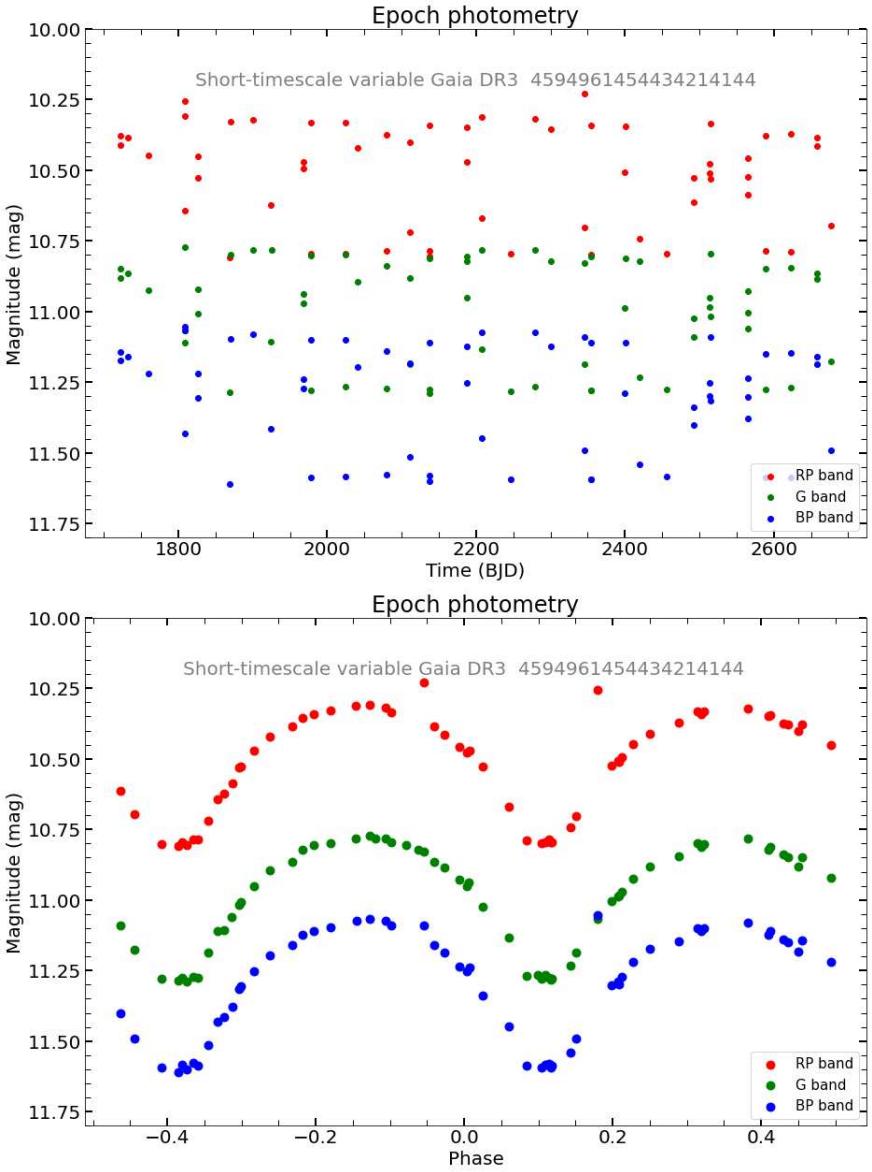

Figure 3.38: Light curve for the short-timescale binary star Gaia DR3 4594961454434214144 in the time domain (top) and in the phase domain (bottom).

3.9 Long period variables

Long period variables (LPV) are typically stars from the asymptotic giant branch (AGB) and the red giant branch (RGB) who show large variability amplitudes, in particular in the visual range, and periods ranging from a few tens of days to 1000 d (Lebzelter et al. 2022 [24]).

Mira is considered the prototype of this type of variable stars. The Gaia DR3 catalogue contains 1 720 558 LPV candidates, but only one of them is included in the all-sky PLATO Input Catalogue, which by default rules out giant stars.

This source, identified as Gaia DR3 3005222633152619904 and EM* AS 119, is a cool, carbon-rich T Tauri giant star of spectral type B3IV[e].

B[e] stars present larger infrared flux excesses due to radiation from their circumstellar disk; this source has been likely included in the PIC due to its high extinction[14].

Its time series in the Gaia photometric bands and its phase-folded light curve according to the tentative period P = 100 d are reported in figure 3.39.

[14]The value of the reddening for this source is $A_V = 2.7$ mag and was determined for the first time by L. Cidale, J. Zorec and L. Tringaniello in the paper available at DOI: `https://doi.org/10.1051/0004-6361:20000409`.

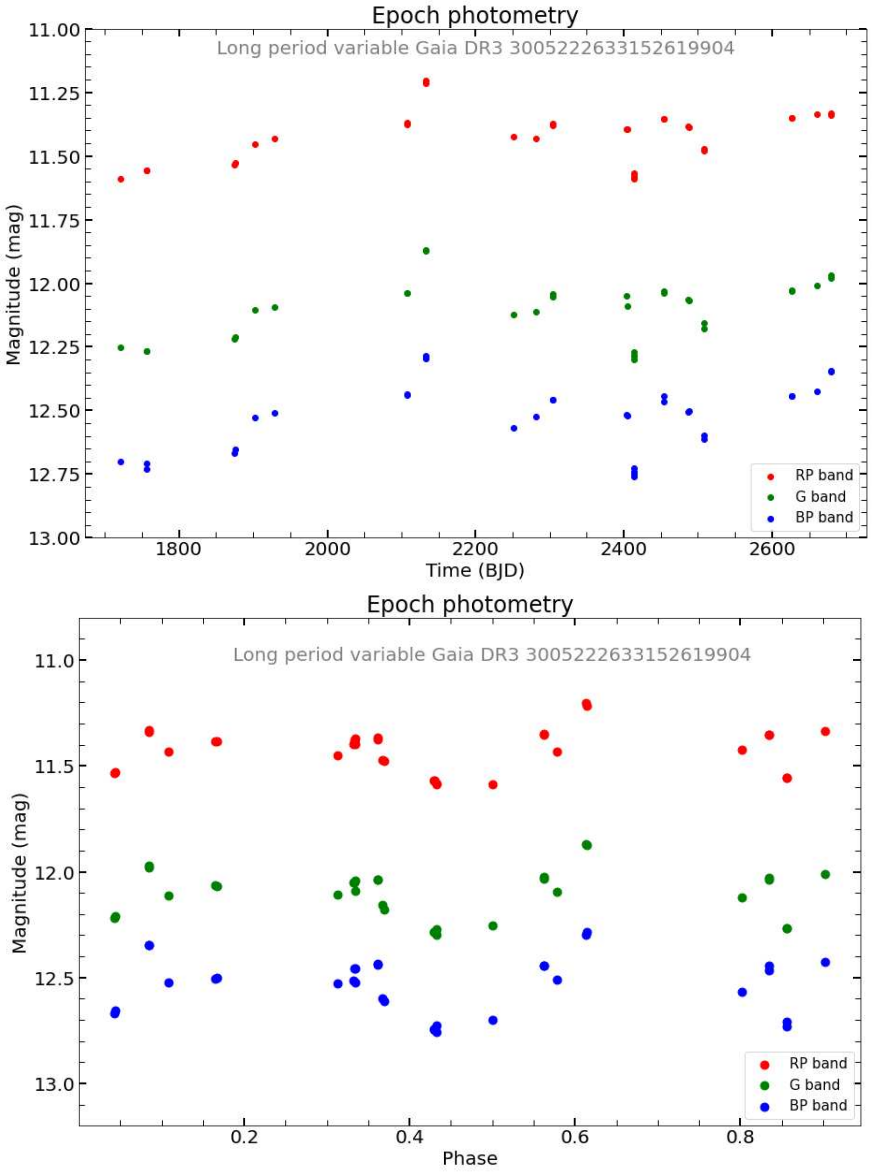

Figure 3.39: Time series (top) and phase-folded lightcurve (bottom) in the G, G_{BP} and G_{RP} bands for the long period variable Gaia DR3 3005222633152619904.

Chapter 4

Conclusions

The ultimate, long-term goal of the exoplanetary research field is to find an Earth-like planet showing possible signatures of life.
The PLATO mission will address the scientific questions concerning the formation and evolution of planets and planetary systems, the uniqueness of our solar system and the existence of potentially habitable small terrestrial planets in long period orbits around bright solar-like host stars.
PLATO will detect transit signals of planets which are bright enough for radial velocity spectroscopy follow up to determine their masses and will provide a unique sample of well characterized "Earth-Sun" analogues. PLATO's target list will be beneficial for future planetary atmosphere spectroscopy with facilities such as JWST, ARIEL, E-ELT, while WEAVE and 4MOST will perform complete spectroscopy of the exoplanet host stars.

Since the flux variability of host stars can challenge the detection and validation of transiting exoplanets, it is of capital importance to interpret and study the variability of all PLATO sources, in order to correctly disentangle stellar and planetary signatures and reliably discriminate false positive astrophysical signals.
This work showed how the PLATO Input Catalogue targets that are distributed in the two outer regions at ecliptic latitudes $\beta > 38°$ (here referred to as LOPN1 and LOPS2), envelop-

ing every allowed choice of the mission observational sky fields, can be distinguished into several classes of variable objects from Gaia Data Release 3, as follows: 7077 short-timescale variables, 6444 eclipsing binaries, 3643 solar-like stars displaying rotational modulation, 591 upper Main Sequence oscillators, 162 RR Lyrae stars, 10 candidate and 495 confirmed exoplanet hosts, 1 Cepheid star and 1 Long Period Variable.

PLATO's observations and ground based program will allow to confirm the candidate transiting extra-solar planets in the Catalogue and characterize those already validated; through timing analysis it will also be possible to detect additional hidden companions in these planetary systems. The final estimated planet yield for the mission for all radii and orbital periods around stars brighter than V = 13 is about 4600.

Eclipsing binaries are among the most interesting variable targets for the PLATO mission; aside from allowing the determination of stellar radii, masses and distances, their prolonged observation will provide insights concerning the distribution of circumbinary planets (CBPs) and the rate of astrophysical false positive detections.
As stated in Desidera et al. 2007 [25], the study of the properties of systems with one (or more) exoplanet orbiting both components of tight or wide stellar binaries is important to improve the current knowledge of planet formation and evolution.
The expected alignment between the planetary and the stellar orbital planes, which strongly increases detection probabilities on eclipsing binaries with near edge-on orbits, make CBPs favourable targets for transit surveys. To date, 217 CBPs have been detected in 154 binary star systems[1] and this number is expected to significantly increase with PLATO.
Moreover, several configurations of eclipsing binaries can mimic a planetary transit signature and generate False Positives (FPs); for instance, a background binary star blended in the same pixels as the bright target star inside PLATO's large window would produce a diluted transit in the target star's lightcurve, comparable to that of a planet.
The vetting of astrophysical false positives will require a variety of ground-based follow-up

[1]For reference: `https://adg.univie.ac.at/schwarz/multiple.html`

filtering observations for PLATO targets, among spectroscopy, imaging, and photometry. The accurate estimate of the number of background contaminants from EBs for PLATO targets, of the overall false-alarm rate and of the dilution factor is open to further research and investigation.

Among our sample, most of the sources that present fast brightness variations are EBs and compact binaries such as X-rays binaries and Cataclismic Variables that are affected by accretion phenomena. PLATO's all-sky accessibility, optical photometry, and rapid observing cadence of 25 and 2.5 seconds for the normal and fast cameras will allow accurate studies for these short timescale targets. PLATO will provide therefore new insights into the field of fast astronomical variability and is set to detect extra-solar planets orbiting compact systems.

The sample of solar-type rotators included in the PLATO Input Catalogue which display flux variability produced by activity cycles, transients (flares) and rotational modulation are of particular relevance for several scientific issues. In the first place, stellar magnetic or chromospheric activity can make transits detection and radial velocity measurements more challenging and, by mimicking their signatures, constitute a source of false positives (Simpson et al. 2022 [26]). Such phenomena as spots, faculae, granulation, and oscillations can induce spurious velocities, referred to as astrophysical noise or stellar jitter, that may mask (or mimic) the Doppler wobble of a planetary companion. Similarly, the occultation of stellar spots by transiting planets may lead to inaccurate estimates of transit parameters.
Moreover, PLATO's long time series will allow the study of magnetic activity cycles and spot decay time, improving the current dynamical stellar evolution models and unveiling a more detailed picture of magnetohydrodynamics of solar-like rotating stars.

PLATO is expected to reveal new features of classical pulsators that will lead to a better understanding of the underlying physical processes, and their influences on stellar evolution.

Certain classes of pulsating variables such as Delta Scuti, Cepheids and RR Lyrae stars lie

on the instability strip on the HR diagram, where the narrow temperature range corresponds to the temperatures at which partial ionisation zones in the star's interior can sustain stellar oscillations.

PLATO will be the first mission to make systematic use of asteroseismology to characterise planet host stars in order to link planetary and stellar evolution. The core program focuses on stars showing oscillations similar to those of the Sun, which are intrinsically stable and excited stochastically by the near-surface convection. The δ Scuti stars in our sample, which are high-mass main sequence pulsators of spectral type F, are some of the best targets for asteroseismology. As for distance indicators such as Cepheids and RR Lyrae stars, their regular pattern of self-excited oscillations can be also exploited with the method of Transit Time Variations (TTV) to search for exoplanetary companions.

Beyond its main scientific objectives, PLATO will be a ground-breaking mission that will sample a wide variety of time-variable phenomena in various populations of the Galaxy and drastically improve the current knowledge on several astrophysical domains.

Appendix A

Detecting and characterizing extra-solar planets and their host stars

Wherever not otherwise specified, the reference for this Appendix is Perryman 2018 [27].

A.1 Photometric transits

The main goal of PLATO is to detect and characterise exoplanets with the transit method, which consists in the detection of the dimming of the stellar flux by an orbiting planet passing through the line-of-sight to Earth and allows to measure the size of the planet with respect to the star.

The probability to observe a transiting planet, although small, is maximized for an inclination i of the orbital plane with respect to line-of-sight of 90° (edge-on orbit); moreover the measure of the transit period allows to derive the size of the orbit, while from the secondary eclipse the eccentricity of the orbit can be retrieved.

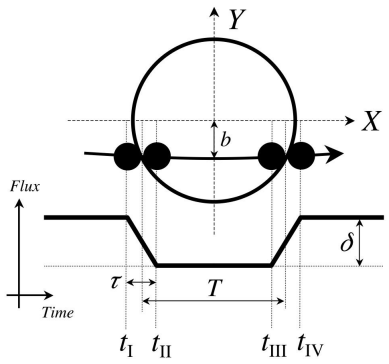

Figure A.1: Model transit light curve. Credits to *Winn [2010]*

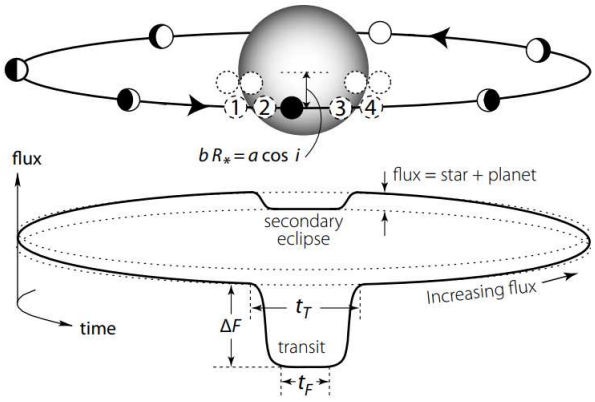

Figure A.2: Schematic illustration of a transiting planet depicting the primary transit and the secondary eclipse. Credits to *Perryman [2011]*

The photometric signal, that is the transit depth corresponding to the fractional decrease of stellar brightness, is proportional to the square of the radius of the planet relative to the radius of the star

$$\delta = \frac{\Delta F}{F} = (\frac{R_P}{R_*})^2, \tag{A.1}$$

therefore the transit method allows to measure directly a planet's size once the size of the host star is known from asteroseismology.

Furthermore from satellite photometry, in sinergy with ground-based radial velocity spectroscopy constraining the planetary mass, the mean bulk density can be obtained. Therefore a mission such as PLATO will be able to fully characterize the targeted extrasolar planets, determining their radius, age, mass and bulk density.

A.2 Radial velocity

Ground-based radial velocity follow-up observations of exoplanetary candidates are a major objective for the PLATO mission.

Periodic Doppler shifts of the stellar spectral features allow to measure the wobbling of the star due to the gravitational influence of the planetary companion around the center of mass of the system.

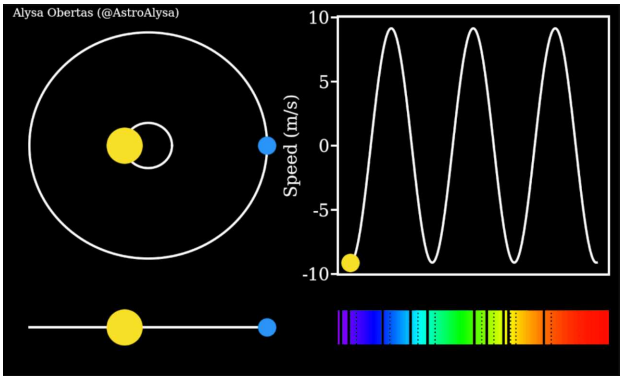

Figure A.3: Radial velocity curve via Doppler spectroscopy. Credits to *Alysa Obertas [2022]*

From the measurement of the semi-amplitude K of the computed stellar radial velocity curve the planet mass relative to the stellar mass times sin$i$ (the "minimum mass" of the planet) can be obtained:

$$K = (\frac{2\pi G}{P})^{1/3} \frac{M_P \sin i}{(M_* + M_P)^{2/3}} \frac{1}{\sqrt{1-e^2}} \tag{A.2}$$

This equation can be written also as:

$$\frac{M_P \sin i}{M_J} = 4.919 \times 10^{-3} \frac{K}{ms^{-1}} (1-e^2)^{1/2} (\frac{P}{d})^{1/3} (\frac{M_P + M_*}{M\odot})^{2/3} \tag{A.3}$$

and for $M_P << M_*$ and $e \approx 0$ the sinusoidal radial velocity signal is given by:

$$K = 28.4 ms^{-1} (\frac{P}{yr})^{-1/3} (\frac{M_P \sin i}{M_J}) (\frac{M_*}{M\odot})^{-2/3} \tag{A.4}$$

Once the planetary mass has been assessed in combination with photometric measure-

ments, the mean density can be retrieved and the rocky or gaseous nature of the planet can be determined.

Precise radial velocity measurements require a large number of spectral absorption lines, thus cooler, later-type stars are preferred targets with respect to hotter stars.
The detection of an Earth-like planet orbiting at 1 AU a true Sun-analogue is beyond the current technological capabilities, but PLATO shall observe stars bright enough to allow for a determination through radial velocity measurements of the mass of a terrestrial planet orbiting a G0V star at distances up to the stellar habitable zones with an accuracy of 10% or better for V = 11 mag.

A.3 Asteroseismology

PLATO will be able to observe up to 50% of the sky to allow for asteroseismology analysis of several thousands of stars at different stages of their evolution and different locations in the sky, with the aim of determining their masses, radii and ages with 10% accuracy.
Asteroseismology is the study of the intrinsic oscillations of stars, which generate small amplitude variations of their light curves and can be used to infer both the internal structure of stars and their bulk properties.
The power spectra of the lightcurves, from which the oscillation frequencies can be obtained, show characteristic spacings between the peaks; these separations provide diagnostic information on the stellar interiors near the core and hence information on the age of the star.
Asteroseismology is part of the core science of PLATO, which will measure the oscillation frequencies of at least 15,000 dwarf and subgiant stars with V<11 mag.

A.4 Astrometry

Astrometry is the astronomical discipline concerned with the accurate measurement and study of the positions and motions of celestial objects.
It has been one of the first techniques used to search for extra-solar planets: the amplitude

of an astrometric signal is sensitive to large mass ratios (massive planets around less massive stars) and increases for exoplanets at large orbital separations and around nearby stars.

Similarly to the spectroscopic technique, astrometric measurements can detect the stellar wobble around the star-plamet system barycenter due to the gravitational perturbation of nearby companions.

The main observable is the angular semi-major axis of the stellar orbit:

$$\alpha = (\frac{M_P}{M_*})(\frac{a}{1AU})(\frac{d}{1pc})^{-1} arcsec, \tag{A.5}$$

where a is the semi-major axis of the planet orbit (here assumed to be circular) and d is the distance of the star from the Sun.

The magnitude of the perturbation induced by a 1 M_J planet in orbit at 5 AU around a 1 M$\odot$ star at a distance of 10 pc from the Sun is 500 μas, for a semi-major axis of 0.01 it is reduced to 1 μas, while an Earth-like planet at 1 AU from its star induces an astrometric signature of 0.3 μas.

Gaia measures the relative separations of the thousands of stars simultaneously present in the combined fields of view following the global astrometry concept in the footsteps of *Hipparcos*: its scanning space astrometry relies on a slowly spinning satellite that measures the crossing times of targets transiting the focal plane.

As a result Gaia's scanning law and wide basic angle allow to obtain absolute parallaxes from differential measurements.

Gaia's full astrometric solution includes the positions on the sky (α, δ), parallax (ω), and proper motion (π) for around 1.46 billion sources, with a limiting magnitude of about G $\approx$ 21 and a bright limit of about G $\approx$ 3.

Gaia parallax accuracies are unprecedented and can reach 7 μas at G = 10, 25 μas at G = 15 and 600 μas at G = 20.

Bibliography

[1] H. Rauer et al. "The PLATO 2.0 mission". In: *Experimental Astronomy* 38.1-2 (2014), pp. 249–330. DOI: 10.1007/s10686-014-9383-4.

[2] Rauer et al. "The PLATO Mission". In: *Astronomische Nachrichten* 337.8-9 (2016), pp. 961–963. DOI: 10.1002/asna.201612408.

[3] ESA Study Team and PLATO Science Team. "PLATO Definition Study Report". In: *ESA-SCI(2017)1*. 2017, pp. 1–139. URL: https://platomission.com/2018/03/08/esa-publications/.

[4] M. Montalto et al. "The all-sky PLATO input catalogue". In: *Astronomy & Astrophysics* 653 (2021), A98. DOI: 10.1051/0004-6361/202140717.

[5] V. Nascimbeni et al. "The PLATO field selection process". In: *Astronomy & Astrophysics* 658 (2022), A31. DOI: 10.1051/0004-6361/202142256.

[6] M. Perryman et al. "GAIA: Composition, formation and evolution of the Galaxy". In: *Astronomy & Astrophysics* 369.1 (Apr. 2001), pp. 339–363. DOI: 10.1051/0004-6361:20010085.

[7] Gaia Collaboration et al. "The Gaia mission". In: *Astronomy & Astrophysics* 595 (2016), A1. DOI: 10.1051/0004-6361/201629272.

[8] L. Eyer et al. "Gaia Data Release 1: The variability processing & analysis and its application to the south ecliptic pole region". In: *arXiv e-prints* (2017). DOI: 10.48550/arXiv.1702.03295.

[9] Gaia Collaboration et al. *Gaia Data Release 3: Summary of the content and survey properties*. 2022. arXiv: 2208.00211 [astro-ph.GA].

[10] L. Eyer et al. *Gaia Data Release 3. Summary of the variability processing and analysis*. 2022. DOI: 10.48550/arXiv.2206.06416.

[11] L. Rimoldini et al. *Gaia Data Release 3. All-sky classification of 12.4 million variable sources into 25 classes*. 2022. DOI: 10.48550/arXiv.2211.17238.

[12] Panagiotis Gavras et al. "Gaia Data Release 3. Cross-match of Gaia sources with variable objects from the literature". In: *Astronomy & Astrophysics* 674 (2023), A22. DOI: 10.1051/0004-6361/202244367.

[13] N. Mowlavi. "Searching transients in large-scale surveys - A method based on the Abbe value". In: *Astronomy & Astrophysics* 568.A78 (2014), p. 38. DOI: 10.1051/0004-6361/201322648.

[14] Bellinger et al. "When a period is not a full stop: Light-curve structure reveals fundamental parameters of Cepheid and RR Lyrae stars". In: *Monthly Notices of the Royal Astronomical Society* 491.4 (2019), pp. 4752–4767. DOI: 10.1093/mnras/stz3292.

[15] R. Townsend. "Photometric modelling of slowly pulsating B stars". In: *Monthly Notices of the Royal Astronomical Society* 330.4 (2002), pp. 855–875. DOI: 10.1046/j.1365-8711.2002.05135.x.

[16] Aviad Panahi et al. "The detection of transiting exoplanets by Gaia". In: *Astronomy & Astrophysics* 663 (July 2022), A101. DOI: 10.1051/0004-6361/202243497.

[17] Gaia Collaboration et al. *Gaia Data Release 3: Stellar multiplicity, a teaser for the hidden treasure*. 2022. arXiv: 2206.05595 [astro-ph.SR].

[18] N. Mowlavi et al. *Gaia Data Release 3. The first Gaia catalogue of eclipsing binary candidates*. 2022. arXiv: 2211.00929 [astro-ph.SR].

[19] Distefano, E. et al. "Gaia Data Release 3. Rotational modulation and patterns of color variations in solar-like variables". In: *A&A* (2022). DOI: 10.1051/0004-6361/202244178.

[20] Gaia Collaboration et al. "Gaia Data Release 3. Pulsations in main-sequence OBAF-type stars". In: *A&A* (2023). DOI: 10.1051/0004-6361/202243767.

[21] Clementini, G. et al. "Gaia Data Release 3. Specific processing and validation of all-sky RR Lyrae and Cepheid stars. The RR Lyrae sample". In: *A&A* (2022). DOI: 10.1051/0004-6361/202243964.

[22] V. Ripepi et al. *Gaia DR3: Specific processing and validation of all-sky RR Lyrae and Cepheid stars – The Cepheid sample*. 2022. arXiv: 2206.06212 [astro-ph.SR].

[23] M. Roelens et al. "Gaia Data Release 2. Short-timescale variability processing and analysis". In: *Astronomy & Astrophysics* 620 (Dec. 2018), A197. DOI: 10.1051/0004-6361/201833357.

[24] Lebzelter, T. et al. "Gaia Data Release 3. The second Gaia catalogue of long-period variable candidates". In: *A&A* (2022). DOI: 10.1051/0004-6361/202244241.

[25] Desidera, S. and Barbieri, M. "Properties of planets in binary systems - The role of binary separation". In: *A&A* 462.1 (2007), pp. 345–353. DOI: 10.1051/0004-6361:20066319.

[26] Emilie R. Simpson et al. "Revisiting BD-06 1339b: A Likely False Positive Caused by Stellar Activity". In: *The Astronomical Journal* 163.5 (2022), p. 215. DOI: 10.3847/1538-3881/ac5d41.

[27] Michael Perryman. *The Exoplanet Handbook*. 2nd ed. Cambridge University Press, 2018. DOI: 10.1017/9781108304160.

[28] EPR-AT. *A European Roadmap for Exoplanets*. ESA, 2010. URL: https://sci.esa.int/s/AGdX6Yw.

[29] ESA and DPAC. *Gaia Data Release 3 Documentation*. ESA, 2023. URL: https://gea.esac.esa.int/archive/documentation/GDR3/index.html.

[30] Exoplanet & Stellar Population Group. 2023. URL: https://groups.dfa.unipd.it/ESPG/plato.html/.

[31] PMC. 2017. URL: https://platomission.com/.

[32] PSM. 2018. URL: https://warwick.ac.uk/fac/sci/physics/research/astro/plato-science.

[33] Nicholas Walton and Gavin Dalton. *Gaia, PLATO and WEAVE: Astrometry, Photometry and Spectroscopy for Exoplanet Characterisation*. PIC Workshop, 2019. URL: https://indico.ict.inaf.it/event/806/.

[34] ESA D/SCI. 2023. URL: https://www.cosmos.esa.int/.

[35] ESA. URL: https://www.esa.int/.

[36] ESA SciTech. 2019. URL: https://sci.esa.int/.

[37] ASI. *Italian Space Agency*. 2023. URL: https://www.asi.it/en/planets-stars-universe/solar-system-and-beyond/plato/.

[38] ESA ESAC. *Gaia Archive*. 2023. URL: https://archives.esac.esa.int/gaia.

[39] NASA and STScI. *MAST*. 2023. URL: https://archive.stsci.edu/index.html.

[40] ASI. *SSDC Sky Explorer*. 2023. URL: https://tools.ssdc.asi.it/.

[41] Unistra/CNRS. *CDS Portal*. 2023. URL: https://cdsarc.u-strasbg.fr/.

[42] CDS. *SIMBAD Astronomical Database*. 2023. URL: http://simbad.u-strasbg.fr/.

[43] CDS. *VizieR*. 2023. URL: https://vizier.cds.unistra.fr/.

[44] Exoplanet Team. *Extrasolar Planets Encyclopaedia*. 2023. URL: http://exoplanet.eu/catalog/.

[45] NExScI. *NASA Exoplanet Archive*. 2023. URL: https://exoplanetarchive.ipac.caltech.edu/index.html.

[46] Mark Taylor. *TOPCAT*. 2017. URL: https://www.star.bristol.ac.uk/mbt/topcat/.

[47] Pierre Raybaut. "Spyder Documentation". In: (2009). URL: https://www.spyder-ide.org/.

[48] Guido Van Rossum and Fred L Drake Jr. *Python Tutorial*. Centrum voor Wiskunde en Informatica Amsterdam, The Netherlands, 1995. URL: http://www.python.org.

[49] Anaconda Software Distribution. *Anaconda Documentation*. Version 2-2.4.0. 2020. URL: `https://docs.anaconda.com/`.

[50] The Overleaf Team. *Overleaf LaTeX editor*. 2014. URL: `https://it.overleaf.com`.